Different Degrees of Partial Melting of the Enriched Mantle Source for Plio−Quaternary Basic Volcanism, Toprakkale (Osmaniye) Region, Southern Turkey

UTKU BAĞCI[1], MUSA ALPASLAN[1], ROBERT FREI[2], MEHMET ALİ KURT[1] & ABİDİN TEMEL[3]

[1] Mersin University, Department of Geological Engineering, Çiftlikköy, TR−33342 Mersin, Turkey
(E-mail: bagciu@mersin.edu.tr)

[2] Geological Institute, University of Copenhagen, Øster Voldgade 10, DK−1350 Copenhagen, Denmark

[3] Hacettepe University, Department of Geological Engineering, Beytepe, TR−06532 Ankara, Turkey

Abstract: The Toprakkale (Osmaniye) region, located in the Yumurtalık fault zone in southern Turkey, contains Quaternary volcanic rocks, shown by their mineralogical and petrographical features to be alkali basaltic and basanitic. These alkaline rocks are enriched in the large ion lithophile elements (LILE) Ba, Th and U, and show light rare earth element (LREE) enrichment relative to heavy rare earth element (HREE) on primitive mantle trace and rare earth element patterns that indicate different partial melting of the same source. The isotopic $^{87}Sr/^{86}Sr$ ratio is relatively low (0.703534–0.703575 for the alkali basalts and 0.703120–0.703130 for the basanites) and the $^{143}Nd/^{144}Nd$ ratio is high (0.512868–0.512877 for the alkali basalts and 0.512885–0.512913 for the basanites), suggesting that both units originated from an isotopically depleted mantle source. The degree of partial melting of the Toprakkale volcanic unit was calculated using the dynamic melting method. The alkali basalts were formed by a high degree of partial melting (9.19%) whereas basanites were formed by a low degree of partial melting (4.58%) of the same mantle source.

All the geochemical evidence suggests that the basic volcanism was generated by decompressional melting under a transtensional tectonic regime in the Yumurtalık fault zone, Southern Anatolia.

Key Words: alkali basalt, basanite, Sr-Nd isotopes, dynamic melting, Yumurtalık fault zone, Turkey

Zenginleşmiş Manto Kaynağının Farklı Oranlardaki Bölümsel Ergimesiyle Oluşan Pliyo−Kuaterner Yaşlı Bazik Volkanizma, Toprakkale (Osmaniye), Güney Türkiye

Özet: Toprakkale (Osmaniye) bölgesi, Yumurtalık fay zonunda yer almakta, mineralojik ve petrografik özelliklerine göre Kuaterner yaşlı alkali bazaltik ve basanitik kayaçlardan oluşmaktadır. Bu alkali kayaçların primitif mantoya göre normalize edilmiş iz ve nadir toprak elementi dağılım desenleri, yüksek iyon çaplı litofil elementlerin (LILE), örneğin Ba, Th ve U ve hafif nadir toprak elementlerince (LREE) ağır nadir toprak elementlerine (HREE) göre zenginleşmesi, benzer bir kökenden farklı bölümsel ergime derecesini göstermektedir. Düşük $^{87}Sr/^{86}Sr$ izotopik değerleri (alkali bazaltlar 0.703534–0.703575; basanitler 0.703120–0.703130) ve yüksek $^{143}Nd/^{144}Nd$ izotopik değerleri (alkali bazaltlar 0.512868–0.512877; basanitler 0.512885–0.512913) alkali bazaltların ve basanitlerin izotopik olarak tüketilmiş manto kaynağından türediğine işaret etmektedir. Toprakkale volkaniklerinin bölümsel ergime derecesi dinamik ergime metodu ile hesaplanmıştır. Alkali bazaltlar yüksek bir bölümsel ergime derecesiyle (9.19%) oluşmuşken, basanitler düşük bir bölümsel erime derecesi (4.58%) sonucu oluşmuşlardır.

Bütün jeokimyasal kanıtlar bazik volkanizmanın Yumurtalık fay zonundaki (Güney Anadolu) transtensiyonal tektonik rejim altında gelişen dekompresyon sonucunda meydana geldiğini işaret etmektedir.

Anahtar Sözcükler: alkali bazalt, basanit, Sr-Nd izotopları, dinamik ergime, Yumurtalık fay zonu, Türkiye

Introduction

Despite the widespread occurrence of intra-continental volcanism, its origin and the nature of its source regions are still controversial. The source of alkali basalts is asthenospheric or lithospheric mantle sources or both (Stein & Hofmann 1992; Stein *et al.* 1997; Shaw *et al.* 2003). Some researchers suggested that lithospheric extension induced decompressional melting (e.g., Turcotte & Emerman 1983; Anderson 1994; King & Anderson 1995, 1998). Others, in contrast, proposed that a mantle plume raised the mantle temperature (e.g., Richards *et al.* 1989; White & McKenzie 1989; Campbell & Griffiths 1990; Vaughan & Scarrow 2003).

The eastern Mediterranean region contains three major strike-slip fault zones: the Dead Sea Fault Zone (DSFZ) and the North and East Anatolian fault zones (NAFZ & EAFZ) (Westaway 1994; Westaway & Arger 1996). Intra-continental basaltic volcanism related to the Dead Sea and East Anatolian fault zones has been extensively studied. These basaltic volcanic rocks are characterized by tholeiitic and alkali olivine basalts (Alıcı *et al.* 2001; Rojay *et al.* 2001) and Polat *et al.* (1997) and Parlak *et al.* (1997, 1998, 2000) suggested that the basaltic volcanism is dominated by alkaline olivine basalts. The Toprakkale volcanic unit dominates along the left-lateral strike-slip Yumurtalık fault zone in southern Turkey (Kelling *et al.* 1987; Kozlu 1987; Karig & Kozlu 1990; Parlak *et al.* 1997, 1998) (Figure 1a). The age of the basaltic volcanism has been determined as younger than 2.25 Ma, based on K-Ar determinations (Arger *et al.* 2000; Tatar *et al.* 2004). Previous studies of the region concentrated on the tectonic evolution of Eastern Turkey, which forms the modern plate boundary zone between the African, Arabian, Eurasian and Turkish plates. The westward movement of the Turkish plate is accommodated by the right-lateral North Anatolian Fault Zone (NAFZ) and the left-lateral East Anatolian Fault Zone (EAFZ) (Nur & Ben-Abraham 1978; Şengör & Yılmaz 1981; Kelling *et al.* 1987; Yılmaz *et al.* 1988; Karig & Kozlu 1990; Perinçek & Çemen 1990; Westaway 1994; Westaway & Arger 1996; Yürür & Chorowicz 1998). Some studies have been concluded on the petrology, geochemistry and K-Ar dating of the basaltic volcanics within these zones (Bilgin & Ercan 1981; Çapan *et al.* 1987; Polat *et al.* 1997; Parlak *et al.* 1997, 1998, 2000; Arger *et al.* 2000; Yurtmen *et al.* 2000, Alıcı *et al.* 2001; Rojay *et al.* 2001). Polat *et al.* (1997) and Parlak *et al.* (1997, 1998, 2000) proposed that alkali olivine basalts in this region were derived from an asthenospheric mantle source, following the lithospheric fractures formed by the strike-slip Dead Sea Fault Zone and the East Anatolian Fault Zone in southern Turkey. Yurtmen *et al.* (2000) suggested that some groups of basalts resemble extension-related alkali basalts; others are similar to ocean island basalts, while yet others show subduction-related characteristics. Alıcı *et al.* (2001) noted the existence in the Karasu valley of both tholeiitic and alkaline basalts, derived from an OIB-like source with the tholeiitic basalts contaminated by some crustal assimilation. In these studies, products of the Toprakkale basaltic volcanism on the Yumurtalık fault zone were not studied in detail, although they included some isotopic and geochronological age determinations.

In this study, we discuss the coexistence of the different basaltic flows, their source-region characteristics, and differences between their degree of partial melting using geochemical data including whole rock major and trace elements, and Sr-Nd isotopes.

Geological Setting

The Çukurova Basin is located in southern Turkey and includes the Adana and İskenderun sub-basins that are separated by the Misis structural high (Kelling *et al.* 1987; Kozlu 1987). These sub-basins were bounded by several NE–SW-trending strike-slip faults at the Maraş triple junction at the convergence of the Anatolian, African and Arabian plates (Şengör & Yılmaz 1981; Kelling *et al.* 1987; Kozlu 1987; Yılmaz *et al.* 1988; Karig & Kozlu 1990; Chorowicz *et al.* 1994). The study area is located in the NE–SW-trending, Miocene to Quaternary İskenderun sub-basin (Figure 1b), that is bordered by the Amanos Mountains to the southeast and the Misis-Andırın complex to the northwest (Albora *et al.* 2006). Originating in the Early Miocene as a deep marine basin, it evolved through a complex tectonic history, involving collision of bordering plates (Early
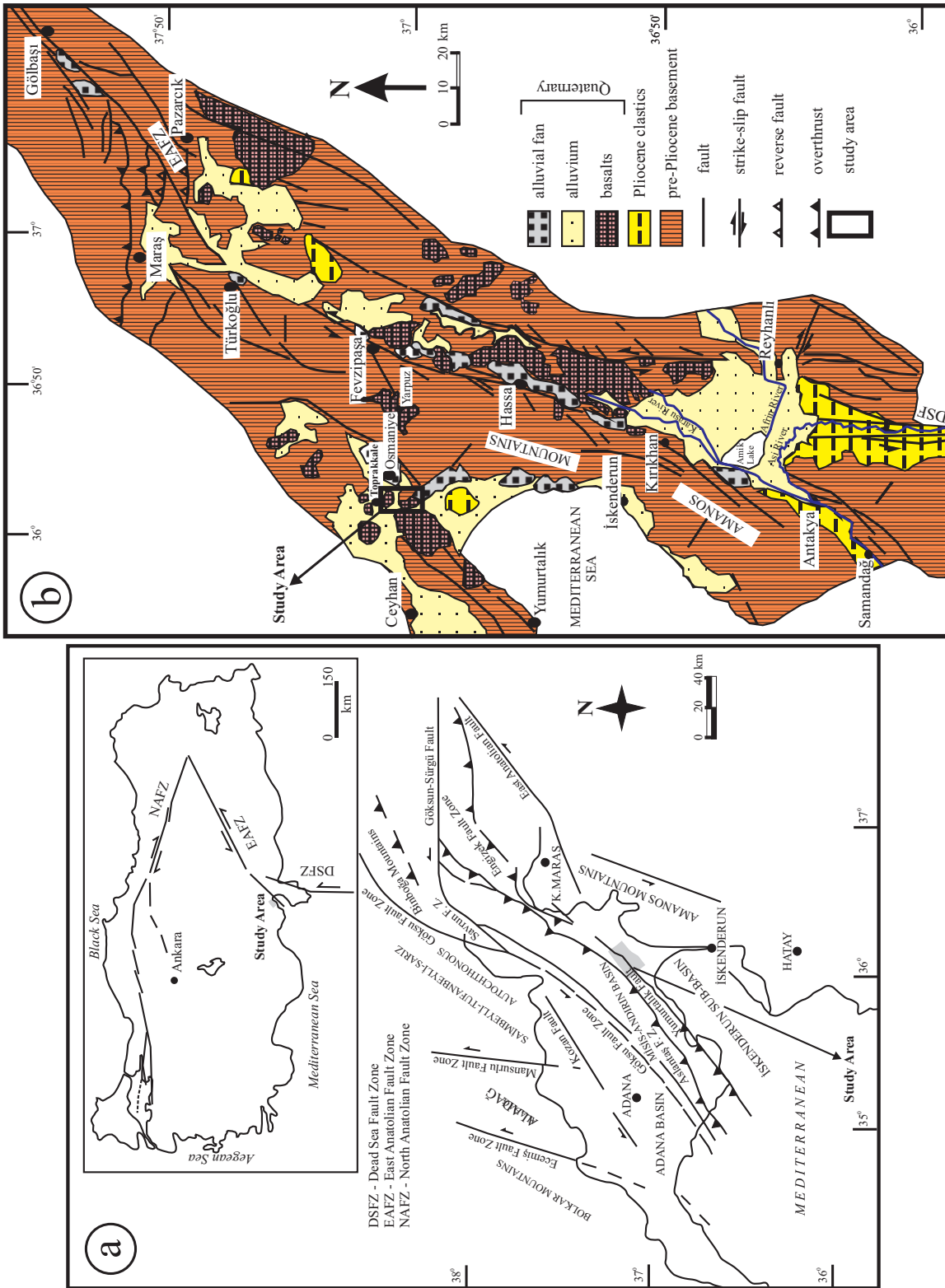
Figure 1. (a) The main tectonic units in the Adana, Misis–Andırın and İskenderun region in southern Turkey (modified from Kozlu 1987); **(b)** simplified geological map of the Toprakkale region and its vicinity (modified from Tolun & Pamir 1975).

Miocene–Early Pliocene) and strike-slip deformation (Plio–Quaternary, Robertson *et al.* 2004). The basin was infilled with turbiditic sediments during the Early Miocene and deltaic sedimentation in the Pliocene–Quaternary (Aksu *et al.* 2005). The Amanos Mountains consist of upper Cretaceous ophiolites, emplaced onto the Arabian platform during the Late Cretaceous (Dilek *et al.* 1999). The Misis-Andırın complex occurs on the northwestern side of the Gulf of İskenderun and is interpreted as an accretionary prism that developed on the northern active margin of the southern Neotethys during the Mid-Eocene to Early Miocene period (Robertson *et al.* 2004).

The Toprakkale volcanic unit generally occurs as massive lava flows. The first eruptive products associated with the unit are lava flows, which yielded K-Ar ages between 2.1 and 2.3 Ma (Arger *et al.* 2000). These flows cover Neogene sedimentary units and occur as massive lava flows 1–2 metres thick. They are found at higher elevations and are recognisable by their dark grey to black colours. The upper parts of the flows contain abundant vesicles. The second eruptive products predominate in the valley bottoms. They consist of three lava flows. The first is thin–medium thick layered, the second is an Aa-type flow, and the third one is a blocky lava flow containing numerous vesicles. Their colours vary from black to grey. Blocky lavas are finer grained than the Aa and thin to medium-thick layered flows. All samples of the Toprakkale volcanic unit are porphyritic and olivine phenocrysts are visible in hand specimen.

Mineralogy and Petrography

The Toprakkale alkali basalts display hypocrystalline, porphyritic intersertal textures with subhedral to anhedral olivine phenocrysts ranging from 0.5 to 2 mm long, plagioclase, clinopyroxene, opaque mineral microlites and small amounts of volcanic glass in the groundmass (Table 1, Figure 2a, b). The olivine phenocrysts are often partly or completely replaced by iddingsite. Some olivine grains are skeletal (Figure 2a) with their rims partially resorbed by melt (Figure 2b). The plagioclase microlites are generally observed to

intersect. Anhedral clinopyroxenes appear to be interstitial within plagioclase microlites (Figure 2a, b). Clinopyroxenes (titanaugite) have a brownish lilac colour in plane polarized light and exhibit weak pleochroism.

The Toprakkale basanites display hypocrystalline, porphyritic intersertal textures and contain subhedral to anhedral olivine phenocrysts. The groundmass is composed of plagioclase, clinopyroxene (titanaugite?), opaque mineral microlites and volcanic glass (Figure 2c, d). The samples taken from blocky lavas show a vitrophyric-porphyritic texture and contain abundant vesicles. Some olivine phenocrysts are sieve-textured (Figure 2c). Plagioclases are commonly seen as microlites although some occur as zoned microphenocrysts (Figure 2d).

Analytical Method

A total of 19 samples were analyzed for major and trace elements at ACME Analytical Laboratories Ltd., Vancouver, Canada. Major element analyses were performed on solutions after $LiBO_2$ fusion and nitric acid digestion of rock powder for inductively coupled plasma-atomic emission spectrometer (ICP-AES). Trace and rare earth element (REE) analyses were determined by an inductively coupled plasma-mass spectrometer (ICP-MS) after $LiBO_2$ fusion and nitric acid digestion. Loss on ignition (LOI) is determined by weight difference after ignition at 1000 °C. Detection limits range from 0.002 to 0.04 wt% for major oxides, 0.1 to 30 ppm for trace elements and 0.05 to 0.1 ppm for the rare earth elements.

A subset of 5 representative samples were analysed by VG Sector 54-IT mass spectrometer for isotopic (Sr and Nd) concentrations at the Danish Isotope Center for Geology (DCIG), University of Copenhagen in Denmark. Sr-Nd isotopic data and concentrations were obtained from 300 mg aliquots of the same powders. For isotope dilution data of Sm and Nd, a mixed ^{147}Sm-^{150}Nd spike was added. Dissolution of the samples was achieved in two successive, but identical steps which consist of a strong 8N HBr attack followed by $HF-HNO_3$, and then by strong HCl. Lead leaching experiments

Table 1. Summary of petrographical and mineralogical features of represantive samples from the Toprakkale volcanic unit.

Sample No	Longitude	Latitude	Rock Series	Phenocryst (%)	Groundmass (%)	Rock Texture
10	37° 2′ 58″	36° 7′ 58″	basanite	Ol (10-15)	Plg+Cpx+Ol+Op+Gl (85-90)	hypocrystalline-porphyritic-intersertal
11	37° 2′ 1″	36° 8′ 12″	basanite	Ol (15-20)	Plg+Cpx+Ol+Op+Gl (80-85)	hypocrystalline-porphyritic-intersertal
12	37° 2′ 1″	36° 8′ 12″	basanite	Ol (10-15)	Plg+Cpx+Ol+Op+Gl (85-90)	hypocrystalline-porphyritic-intersertal
15	37° 2′ 31″	36° 8′ 17″	basanite	Ol (10-15)	Plg+Cpx+Ol+Op+Gl (85-90)	hypocrystalline-porphyritic-intersertal
16	37° 2′ 5″	36° 7′ 45″	basanite	Ol (15-20)	Plg+Cpx+Ol+Op+Gl (80-85)	hypocrystalline-porphyritic-intersertal
17	37° 2′ 5″	36° 7′ 45″	basanite	Ol (10-15)	Plg+Cpx+Ol+Op+Gl (85-90)	hypocrystalline-porphyritic-intersertal
18	37° 2′ 37″	36° 7′ 55″	basanite	Ol (20-25)	Plg+Cpx+Ol+Op+Gl (75-80)	hypocrystalline-porphyritic-intersertal
19	37° 2′ 38″	36° 7′ 55″	basanite	Ol (10-15)	Plg+Cpx+Ol+Op+Gl (85-90)	hypocrystalline-porphyritic-intersertal
20	37° 2′ 39″	36° 7′ 55″	basanite	Ol (10-15)	Plg+Cpx+Ol+Op+Gl (85-90)	hypocrystalline-porphyritic-intersertal
21	37° 2′ 39″	36° 7′ 55″	basanite	Ol (10-15)	Plg+Cpx+Ol+Op+Gl (85-90)	hypocrystalline-porphyritic-intersertal
22	37° 2′ 39″	36° 7′ 55″	basanite	Ol (10-15)	Plg+Cpx+Ol+Op+Gl (85-90)	hypocrystalline-porphyritic-intersertal
23	37° 2′ 42″	36° 7′ 53″	basanite	Ol (5-10)	Plg+Cpx+Ol+Op+Gl (90-95)	hypocrystalline-porphyritic-intersertal
24	37° 2′ 42″	36° 7′ 53″	basanite	Ol (10-15)	Plg+Cpx+Ol+Op+Gl (85-90)	hypocrystalline-porphyritic-intersertal
25	37° 2′ 39″	36° 7′ 51″	basanite	Ol (15-20)	Plg+Cpx+Ol+Op+Gl (80-85)	vitrophyric-porphyritic
26	37° 2′ 44″	36° 07′ 51″	basanite	Ol (15-20)	Plg+Cpx+Ol+Op+Gl (80-85)	hypocrystalline-porphyritic-intersertal
27	37° 2′ 44″	36° 7′ 51″	basanite	Ol (10-15)	Plg+Cpx+Ol+Op+Gl (85-90)	hypocrystalline-porphyritic-intersertal
28	37° 2′ 44″	36° 7′ 51″	basanite	Ol (10-15)	Plg+Cpx+Ol+Op+Gl (85-90)	vitrophyric-porphyritic
13	37° 1′ 43″	36° 8′ 26″	alkali basalt	Ol (15-20)	Plg+Cpx+Ol+Op+Gl (80-85)	hypocrystalline-porphyritic-intersertal
14	37° 2′ 29″	36° 8′ 13″	alkali basalt	Ol (10-15)	Plg+Cpx+Ol+Op+Gl (85-90)	hypocrystalline-porphyritic-intersertal
T-3	30°8′12″	37°2′39″	alkali basalt	Ol (20-25)	Cpx+Plg+Ol+Op+Gl (75-80)	hypocrystalline-porphyritic-intersertal
T-4	30°8′40″	37°2′59″	alkali basalt	Ol (15-20)	Cpx+Plg+Ol+Op+Gl (75-80)	hypocrystalline-porphyritic-intersertal
T-9	30°8′30″	37°1′49″	alkali basalt	Ol (15-20)	Cpx+Plg+Ol+Op+Gl (75-80)	hypocrystalline-porphyritic-intersertal
T-10	30°8′31″	37°1′48″	alkali basalt	Ol (10-15)	Cpx+Plg+Ol+Op+Gl (85-90)	hypocrystalline-porphyritic-intersertal
T-11	30°8′31″	37°1′49″	alkali basalt	Ol (20-25)	Cpx+Plg+Ol+Op+Gl (75-80)	hypocrystalline-porphyritic-intersertal

Ol– olivine, Cpx– clinopyroxene, Plg– plagioclase, Op– opaque, Gl– glass
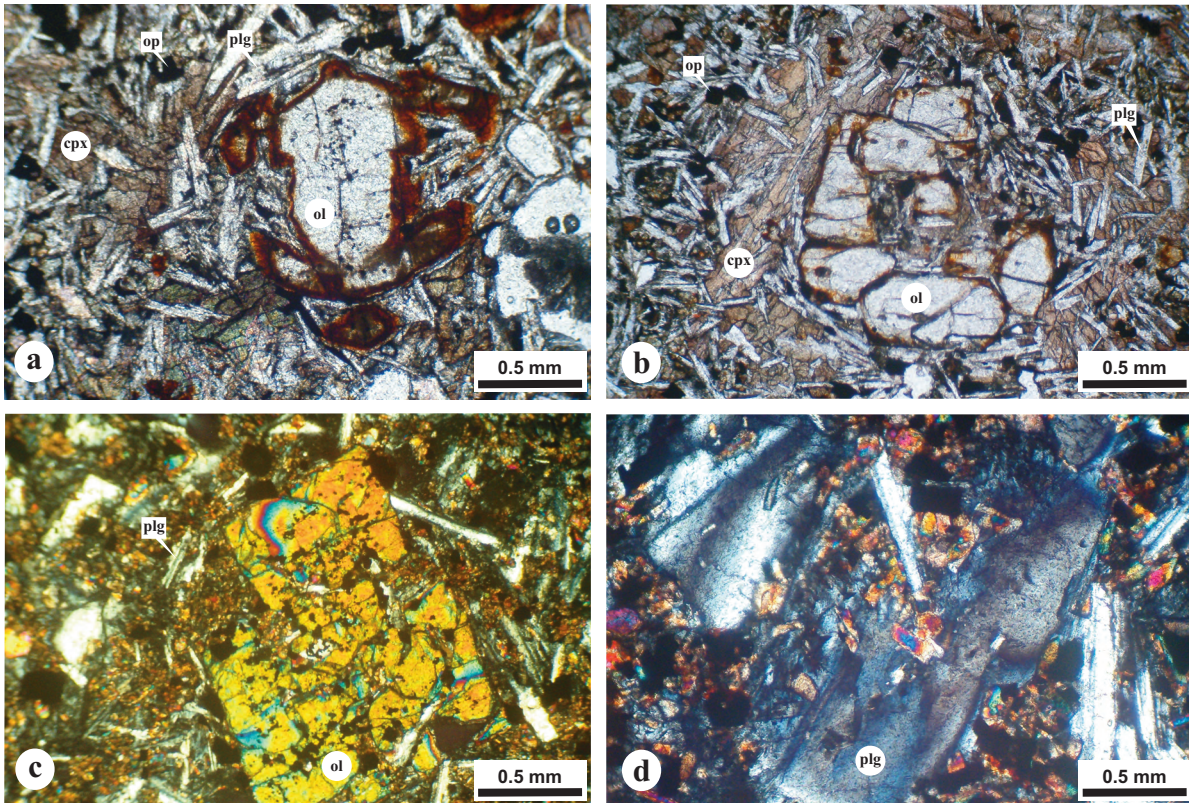
Figure 2. Microphotos for the alkali basalts and basanites from the Toprakkale volcanic unit: **(a)** skeletal growth of olivine phenocryst, **(b)** resorbed olivine phenocryst resorbed by melt, **(c)** sieve-textured olivine phenocryst, **(d)** zoned plagioclase phenocryst; ol– olivine, cpx– clinopyroxene, plg– plagioclase, op– opaque.

involved a 1N HCl attack for 5 minutes, after which the leachate was pipetted off and processed as a separate sample. Chemical separation of Sr and REE from whole-rock samples was carried out on conventional cation exchange columns, followed by separation using HDEHP-coated beads (BIO-RAD) charged in 6 ml quartz glass columns. Purification of the Sr fraction was achieved by a pass over micro-columns containing SrSpecTM resin. REE were further separated over HDEHP-coated bio beads (BioRad) loaded in 6 ml glass stem columns. A Standard HBr-HCl-HNO$_3$ elution recipe was applied for both column steps.

Total Pb procedural blanks were <125 pg for whole-rock chemistry, and are negligible relative to the amount of Pb recovered from each sample. Procedural blanks for Nd (<30 pg) and Sr (<100 pg) are insignificant, and do not influence the measured isotope ratios beyond their respective precisions. Mass spectrometric analyses were carried out on a VG Sector 54-IT instrument at the Geological Institute, University of Copenhagen.

The mean value for our internal JM Nd Standard (referenced against La Jolla) during the period of measurement was 0.511115 for $^{143}Nd/^{144}Nd$, with a 2σ external reproducibility of ± 0.000013 (five measurements). Sr was normalized to $^{86}Sr/^{88}Sr=$ 0.1194, and repetitive analyses of the NBS 987 Sr standard yielded $^{87}Sr/^{88}Sr=$ 0.710248 ± 0.000004 (2s, $n=$ 6).

Geochemistry

The major, trace, REE element contents and normative mineralogy of the Toprakkale volcanic unit are presented in Table 2.

Table 2. Major and trace element contents and normative mineralogy of alkali basalts and basanites from the Toprakkale volcanic unit (major and trace elements are given in wt% and ppm, respectively).

Sample	Basanites																	Alkali basalts						
	10	11	12	15	16	17	18	19	20	21	22	23	24	25	26	27	28	13	14	T-3	T-4	T-9	T-10	T-11
SiO_2	44.29	44.59	44.62	44.4	44.11	44.36	44.37	43.93	44.15	43.8	44.1	44.43	44.01	43.89	44.09	44.27	44.18	46.48	48.11	47.53	47.24	46.74	46.84	47.08
Al_2O_3	15.3	15.51	15.51	15.56	14.8	14.63	14.84	14.88	15.53	14.78	14.8	15.1	15.4	14.67	15.31	15.37	15.06	14.82	15.21	15.42	15.33	15.19	15.55	16.04
tFe_2O_3	13.22	13.03	13.14	13.27	13.36	13.3	13.25	13.31	13.06	13.41	13.31	13.2	13.11	13.57	13.23	13.07	13.16	13.19	13.05	12.47	12.38	12.58	12.78	12.54
MgO	7.5	6.92	6.97	7.06	8.54	8.8	8.39	8.4	7.79	9.11	8.82	8.14	7.75	9.11	7.45	7.73	7.97	8.72	7.77	8.7	9	8.94	8.42	7.47
CaO	10.75	10.77	10.87	10.85	10.39	10.52	10.57	10.49	10.66	10.3	10.58	10.61	10.54	10.28	10.69	10.49	10.75	10.02	10.13	9.43	9.44	9.54	9.49	9.7
Na_2O	3.84	3.74	3.75	3.86	3.62	3.48	3.53	3.72	3.78	3.64	3.5	3.93	3.93	3.47	3.9	4.06	3.38	2.95	3.12	3.14	3.34	3.19	2.97	3.04
K_2O	1.45	1.47	1.47	1.43	1.46	1.39	1.4	1.47	1.47	1.33	1.39	1.21	1.37	1.46	1.46	1.31	1.49	0.83	0.71	0.71	0.76	0.83	0.7	0.69
TiO_2	2.86	2.92	2.93	2.93	2.82	2.77	2.82	2.8	2.91	2.83	2.8	2.88	2.92	2.78	2.89	2.83	2.88	2.01	1.88	1.93	1.92	1.99	1.88	1.91
P_2O_5	0.93	0.91	0.89	0.9	0.92	0.88	0.91	0.9	0.91	0.92	0.88	0.92	0.91	0.91	0.93	0.91	0.95	0.39	0.34	0.312	0.306	0.359	0.315	0.31
MnO	0.16	0.16	0.16	0.16	0.16	0.16	0.16	0.16	0.16	0.16	0.16	0.16	0.16	0.16	0.16	0.16	0.16	0.16	0.15	0.16	0.16	0.16	0.17	0.16
Cr_2O_3	0.02	0.017	0.017	0.017	0.026	0.026	0.025	0.025	0.02	0.029	0.027	0.023	0.02	0.03	0.019	0.02	0.025	0.037	0.034	0.045	0.045	0.045	0.048	0.04
LOI	0.1	0.1	0.1	0.1	0.1	0.1	0.1	0.1	0.1	0.1	0.1	0.1	0.1	0.1	0.1	0.1	0.1	0.3	0.1	-0.2	-0.3	0.1	0.5	0.7
Total	100.42	100.14	100.43	100.54	100.31	100.42	100.37	100.19	100.54	100.41	100.47	100.70	100.22	100.23	100.23	100.32	100.11	99.91	100.60	99.65	99.62	99.66	99.66	99.68
Ni	84	74	68	80	133	137	138	127	81	152	143	101	88	151	90	86	118	149	101	126	138	150	151	119
Sc	25	25	25	25	25	24	24	25	25	24	25	25	25	24	25	25	26	24	23	23	22	23	22	23
Ba	314.4	296.3	312.1	319.5	315.7	337.4	330.2	320.5	340.8	321	310.5	327.4	323.6	333.5	320.8	322.2	359.2	188.8	186.4	195	185	167	182	186
Co	52.1	51.4	47.8	48.7	54.7	56.2	57.6	54.7	55.4	57.6	57.1	56.2	51.1	59.5	50.6	52.1	52	54.5	55.7	72.3	73.4	68.7	64.9	63.9
Cs	0.2	0.2	0.2	0.1	0.2	0.2	0.2	0.3	0.1	0.1	0.2	0.2	0.2	0.1	0.1	0.3	<1	0.2	<1	<1	<1	0.1	<1	<1
Ga	22.7	23.4	22.4	22.8	22.5	22.9	23.5	22.3	23.6	22.9	21.8	22.9	22.7	22.2	22.9	22.9	23.3	22.1	23.2	18	19.2	19	19.6	19.5
Hf	4	4.4	4.6	4.2	4.6	4	4.5	4.3	4.3	4.1	4.2	4.5	4.6	4.3	4.1	4.4	4.6	3.2	2.6	2.7	2.8	2.8	2.7	2.7
Nb	47.1	46	46.7	48.1	48.7	48	50.5	47.7	49.6	50.7	45.1	50.2	49.4	48.1	47.7	48.1	51.3	22.2	17.7	15.9	16.7	19.4	16.3	16.8
Rb	15.5	14.9	15.1	15.4	15.4	15	16.3	15.4	14	14	15.4	16.2	15.8	15.7	15.7	14.5	16.1	9.8	7.3	5.5	7.6	8.5	6.5	6.3
Sr	975.5	955.7	974.2	975.2	970.6	997.2	1014.1	998.4	992.1	992.9	958.4	1015	994.5	999	989.6	986.7	1053.3	548.7	530.3	521.1	579	573.9	526.5	534.7
Ta	2.6	2.6	2.7	2.5	2.5	2.7	2.6	2.7	2.6	2.6	2.5	2.6	2.5	2.5	2.6	2.7	2.8	1.2	1	0.9	1	1.2	1	1
Th	3	2.9	3.1	2.8	2.7	3.3	3.2	2.7	2.7	3.3	3.3	3.5	3.1	3.3	3.4	3.1	3.9	2.7	2	2.3	2.2	2.2	1.9	2.1
U	0.9	0.9	0.9	0.9	1	0.9	1	0.9	0.9	1	0.9	1	0.8	0.9	0.9	0.9	1	0.7	0.5	0.4	0.5	0.5	0.6	0.5
V	237	235	244	247	235	238	242	237	250	237	237	238	242	229	239	238	240	216	213	203	207	205	202	207
Zr	176.3	174.2	179.4	181.4	177.4	176.6	184.4	179.7	184.9	184.2	171.1	183.5	181.1	176.6	179.1	183.3	189.4	123.5	112.9	101.7	105.8	111.3	103.4	107
Y	27.6	28.2	28.5	28.2	27.3	27.4	27.3	27.2	28.2	27.5	26	28.5	27.5	26.8	27.9	28	28.1	22.1	22.8	18.8	19.3	19.9	19.5	20
La	37.9	37.7	37.3	38.4	38	38.2	39.7	39.1	39.1	38.7	36.3	39	38.5	38.2	38.4	38.6	41.9	22.4	21.1	19.3	20.9	20.3	19.1	19.5
Ce	80.4	82	79.2	82.4	81.3	80.9	85.8	83.2	83.7	82.5	78	83.7	82	81.3	81.4	81.6	90.6	46.7	42.3	36.2	37.7	40.8	36.7	37.3
Pr	9.3	9.23	8.97	9.4	9.33	9.2	9.53	9.4	9.49	9.28	8.98	9.56	9.34	9.39	9.28	9.37	10.07	5.09	4.82	4.56	4.78	4.97	4.6	4.68
Nd	36.6	37.9	37.5	38.7	38.5	38.1	38	37.6	39.4	36.5	37	38.6	39.5	38.4	37.9	38.6	41.8	21.9	20.3	19.3	19.9	20.5	19.1	18.7
Sm	8.1	8	7.7	8.3	8.5	8	8.4	7.8	8.1	8.3	7.5	8.2	8.3	7.9	7.9	8.2	8.6	5.2	4.6	4.21	4.33	4.48	4.16	4.3
Eu	2.66	2.6	2.78	2.82	2.7	2.64	2.74	2.69	2.74	2.69	2.61	2.77	2.72	2.59	2.72	2.77	2.84	1.71	1.73	1.55	1.58	1.65	1.54	1.63
Gd	6.48	7.13	6.99	6.99	6.76	6.73	6.83	6.52	6.97	6.74	6.31	7.06	7	6.71	6.97	6.96	7.5	5.06	4.49	4.32	4.38	4.47	4.33	4.36
Tb	1.06	1.05	0.99	1.04	1.05	1	1.03	0.99	1.04	1	0.99	1.07	1.05	1	1	1.08	1.09	0.79	0.73	0.71	0.76	0.73	0.72	0.72
Dy	4.94	5.06	5.28	5.29	4.84	5.22	5.32	4.99	5.45	5.12	4.96	5.32	5.29	5.16	5.17	5.39	5.2	4.04	3.99	3.6	3.69	3.62	3.63	3.8
Ho	1.01	0.96	0.97	1.04	0.98	0.98	1.05	1	0.99	0.96	0.92	1.04	1.01	0.97	1.02	1.02	1.04	0.81	0.79	0.73	0.73	0.71	0.69	0.74
Er	2.33	2.31	2.41	2.37	2.28	2.32	2.26	2.32	2.36	2.3	2.16	2.33	2.36	2.28	2.35	2.36	2.34	1.95	1.93	1.85	1.87	1.83	1.8	1.88
Tm	0.33	0.33	0.32	0.36	0.3	0.34	0.35	0.33	0.34	0.3	0.35	0.34	0.32	0.35	0.37	0.33	0.34	0.28	0.28	0.27	0.28	0.26	0.26	0.28
Yb	2.07	2.11	2.02	1.96	2.02	1.93	2.06	2.21	2.22	2.02	1.96	2.07	2.12	1.98	2.09	2.21	2.14	1.71	1.72	1.56	1.52	1.49	1.55	1.59
Lu	0.28	0.28	0.3	0.28	0.27	0.26	0.31	0.27	0.27	0.27	0.25	0.31	0.28	0.28	0.3	0.3	0.3	0.24	0.26	0.22	0.23	0.23	0.22	0.24
Pb	1	1.5	1.7	1.1	1.5	1.6	1.4	1.5	1.3	1.1	1.9	1.2	1.2	1.7	1.2	1.3	2.1	1.9	1.9	2.1	2.1	1.8	1.7	1.1
Nb/U	52.33	51.11	51.89	53.44	48.70	53.33	50.50	53.00	55.11	50.70	50.11	50.20	61.75	53.44	53.00	53.44	51.30	31.71	35.40	39.75	33.40	38.80	27.17	33.60
La/Nb	0.80	0.82	0.80	0.80	0.78	0.80	0.79	0.82	0.79	0.76	0.80	0.78	0.78	0.79	0.81	0.80	0.82	1.01	1.19	1.21	1.25	1.05	1.17	1.16
Ba/Nb	6.68	6.44	6.68	6.64	6.48	7.03	6.54	6.72	6.87	6.33	6.88	6.52	6.55	6.93	6.73	6.70	7.00	8.50	10.53	12.26	11.08	8.61	11.17	11.07
Ce/Pb	80.40	54.67	46.59	74.91	54.20	50.56	61.29	55.47	64.38	75.00	41.05	69.75	68.33	47.82	67.83	62.77	43.14	24.58	22.26	17.24	17.95	22.67	21.59	33.91
K/Nb	255.55	265.27	261.29	246.79	248.86	240.38	230.13	255.82	246.02	217.76	255.84	200.08	230.21	251.96	254.08	226.08	241.10	310.35	332.98	370.67	377.77	355.15	356.48	340.93
Or	8.57	8.69	8.69	8.39	8.63	8.21	8.27	8.69	8.63	7.86	8.21	7.09	8.10	8.63	8.63	7.74	8.81	4.90	4.20	4.20	4.49	4.90	4.20	4.14
Al	11.50	13.17	12.55	11.99	11.49	12.02	12.40	10.47	11.04	11.10	11.06	12.88	11.55	10.78	11.12	12.32	12.02	21.75	26.07	25.99	23.96	22.87	25.22	25.98
An	20.14	21.19	21.05	20.83	19.78	20.13	20.45	19.53	21.02	20.00	20.48	19.86	20.28	20.08	19.90	19.81	21.52	24.86	25.25	25.92	24.65	24.78	27.25	28.38
Ne	11.33	10.01	10.34	11.11	10.32	9.40	9.42	11.38	11.25	10.63	10.01	10.95	11.76	10.02	11.85	11.89	8.98	1.79	0.13	0.36	2.33	2.32	0.09	0.00
Di	22.04	21.52	22.03	21.99	20.89	21.29	21.10	21.66	20.98	20.28	21.21	21.63	21.23	20.20	22.07	21.38	20.88	18.36	18.45	15.43	16.44	16.64	16.48	14.91
Ol	15.05	13.99	13.94	14.21	17.53	17.83	17.07	17.01	15.70	18.78	17.86	16.24	15.65	19.01	14.95	15.62	16.30	19.75	17.79	20.10	20.17	20.18	20.37	17.96
Mt	3.83	3.78	3.80	3.83	3.87	3.84	3.83	3.86	3.77	3.87	3.84	3.80	3.80	3.93	3.83	3.78	3.81	3.84	3.77	3.62	3.60	3.67	3.74	3.67
Il	5.41	5.55	5.55	5.55	5.34	5.24	5.34	5.32	5.51	5.36	5.30	5.43	5.55	5.26	5.49	5.36	5.47	3.84	3.55	3.67	3.65	3.80	3.61	3.67
Ap	2.15	2.11	2.06	2.09	2.13	2.04	2.11	2.09	2.11	2.13	2.04	2.11	2.11	2.11	2.15	2.11	2.20	0.90	0.79	0.72	0.72	0.83	0.74	0.72

tFe_2O_3 represents total iron oxide as ferric iron; LOI, loss on ignition

All the samples from the Toprakkale region plotted in basalt and basanite fields on a total alkali - silica diagram (Le Maitre *et al.* 1989). Samples of the first eruptive products are seen on the dividing line between alkali and sub-alkali fields (Figure 3). These samples have normative nepheline and hence an alkaline character (Table 2).
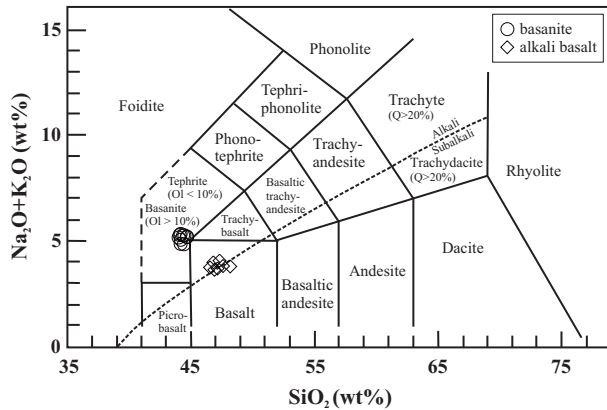
Figure 3. Total alkali - silica diagram (Le Maitre *et al.* 1989) of alkali basalts and basanites from the Toprakkale volcanic rocks. Dashed line dividing the alkali and subalkali fields is from Irvine & Baragar (1971).

Both volcanic units can be easily distinguished from each other in major and trace element contents. Plots of MgO versus major and selected trace elements are shown in Figures 4a–h & 5a–j. Major element variations against MgO indicate that the CaO and Al_2O_3 are negatively correlated while Fe_2O_3 is positively correlated (Figure 4a–h). Trace element variations versus MgO contents do not show any correlation (Figure 5a–h), whereas Cr and Ni are positively correlated with MgO (Figure 5i, j).

The primitive mantle normalized trace element patterns are shown for both volcanic units in Figure 6. The basanites have the highest relative enrichment in highly and moderately incompatible trace elements; the alkali basalts have less enriched patterns than the basanites.

The basanites show distinct positive anomalies for Ba, Nb (and Ta), La and Ce, and negative anomalies for Th, U, K and Pb (Figure 6a) resulting in high ratios of Ce/Pb (17.24–80.40), Nb/U (27.17–61.75) and low K/Nb (200.08–377.77), relative to

primitive mantle (Sun & McDonough 1989). Although the alkali basalts display trace element patterns which are enriched in highly and moderately incompatible trace elements, they generally have a positive Pb anomaly in Figure 6b, although one sample has a negative Pb anomaly. Positive Pb anomalies, along with low Nb-Ta concentrations for basaltic rocks can be attributed to crustal assimilation processes (Wilson 1989). Both volcanic units have slightly positive Sr anomalies (Figure 6a, b). Although both volcanic units have fractionated REE patterns, those of basanites are more fractionated than those of the alkali basalts (Figure 6c). Both units have small positive Eu anomalies (Figure 6c). Fractionated REE patterns for basanites and alkali basalts are consistent with derivation from a mantle source containing residual garnet resulting in high La/Yb_N ratios (12.53–14.2 for basanites and 8.80–9.86 for alkali basalts, Figure 6c) (Shimizu & Kushiro 1975; Wood 1979). Differences between REE patterns of the basanites and alkali basalts possibly reflect the different degrees of partial melting of a single mantle source, or melting from different source regions.

Sr-Nd Isotopes

The Sr and Nd isotopic composition for the Toprakkale volcanic unit are given in Table 3. The $^{87}Sr/^{86}Sr$ isotopic ratio is low (0.703534–0.703575 for the alkali basalts and 0.703120–0.703130 for the basanites) and the $^{143}Nd/^{144}Nd$ ratio is high (0.512868–0.512877 for the alkali basalts and 0.512885–0.512913 for the basanites). The $^{87}Sr/^{86}Sr$ - $^{143}Nd/^{144}Nd$ diagram shows that all samples are depleted in $^{87}Sr/^{86}Sr$ and plot in the depleted quadrant of mantle array (Figure 7). Basanites have more depleted Sr isotopic ratios than the alkali basalts (Figure 7 & Table 3). Basanites plot within the Sr-Nd range of the Kula volcanics (Alıcı *et al.* 2002) (Figure 7) whereas the alkali basalts plot outside the areas previously defined for Plio-Quaternary volcanics of the Kula region (Alıcı *et al.* 2002), northwest Anatolia (Aldanmaz *et al.* 2006) and NW Harrat Ash Shaam, Israel (Weinstein *et al.* 2006). (Figure 7). The alkali basalts have enriched Sr isotopic ratios and depleted Nd isotope ratios.
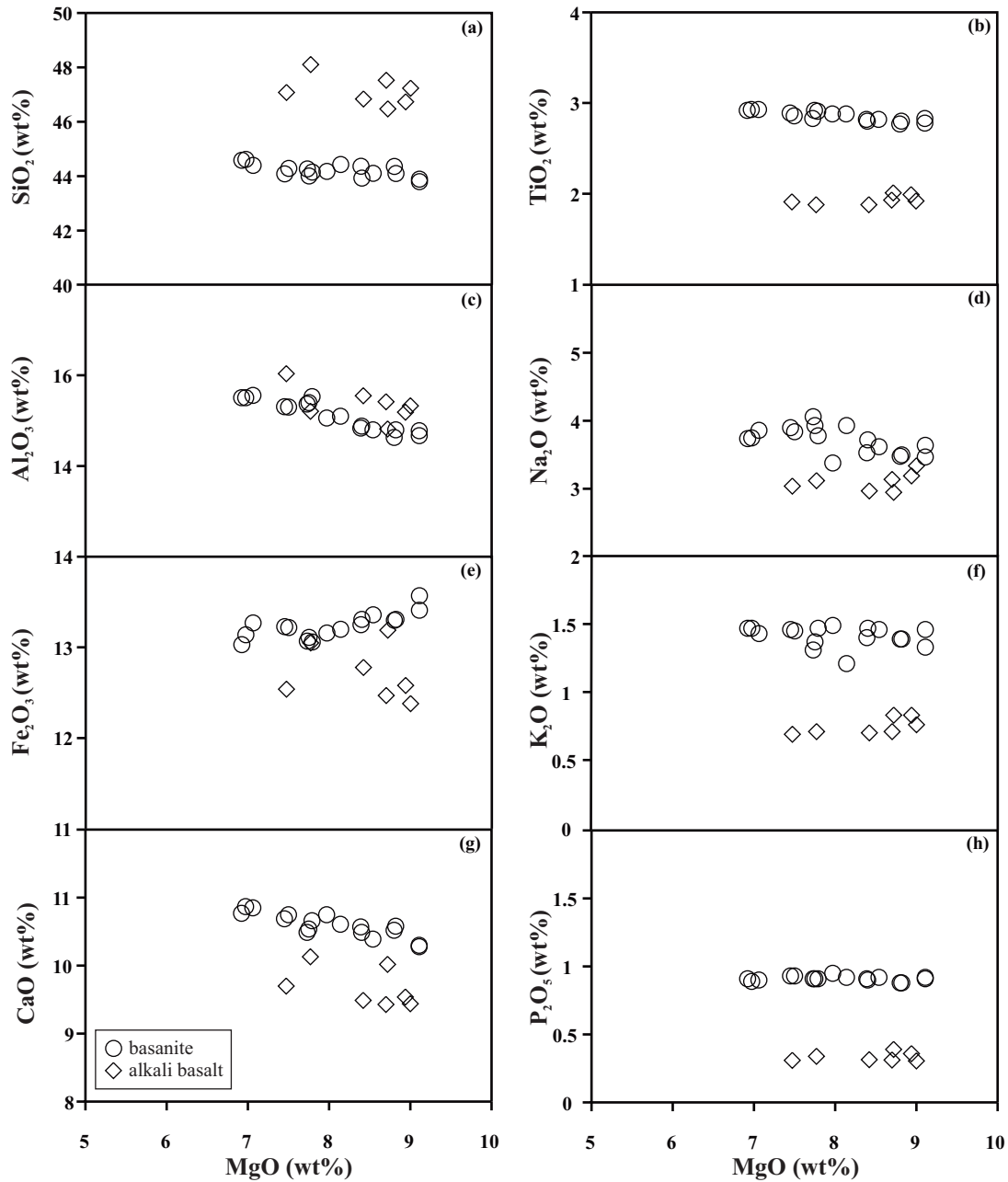
Figure 4. Major element variation diagrams of alkali basalts and basanites from the Toprakkale volcanic unit.

Discussion

Geochemical and isotopic characteristics of the Toprakkale basanites and alkali basalts differ from each other. Basanites have a narrow compositional range but alkali basalts have a limited compositional range. These features may originate from magmatic processes such as assimilation, fractionation and partial melting, which acted on the evolution of these units. Large differences between the geochemical characteristics of both units can also be generated by the differences of the mineralogies of the source regions for these two melts. Therefore, crustal

123
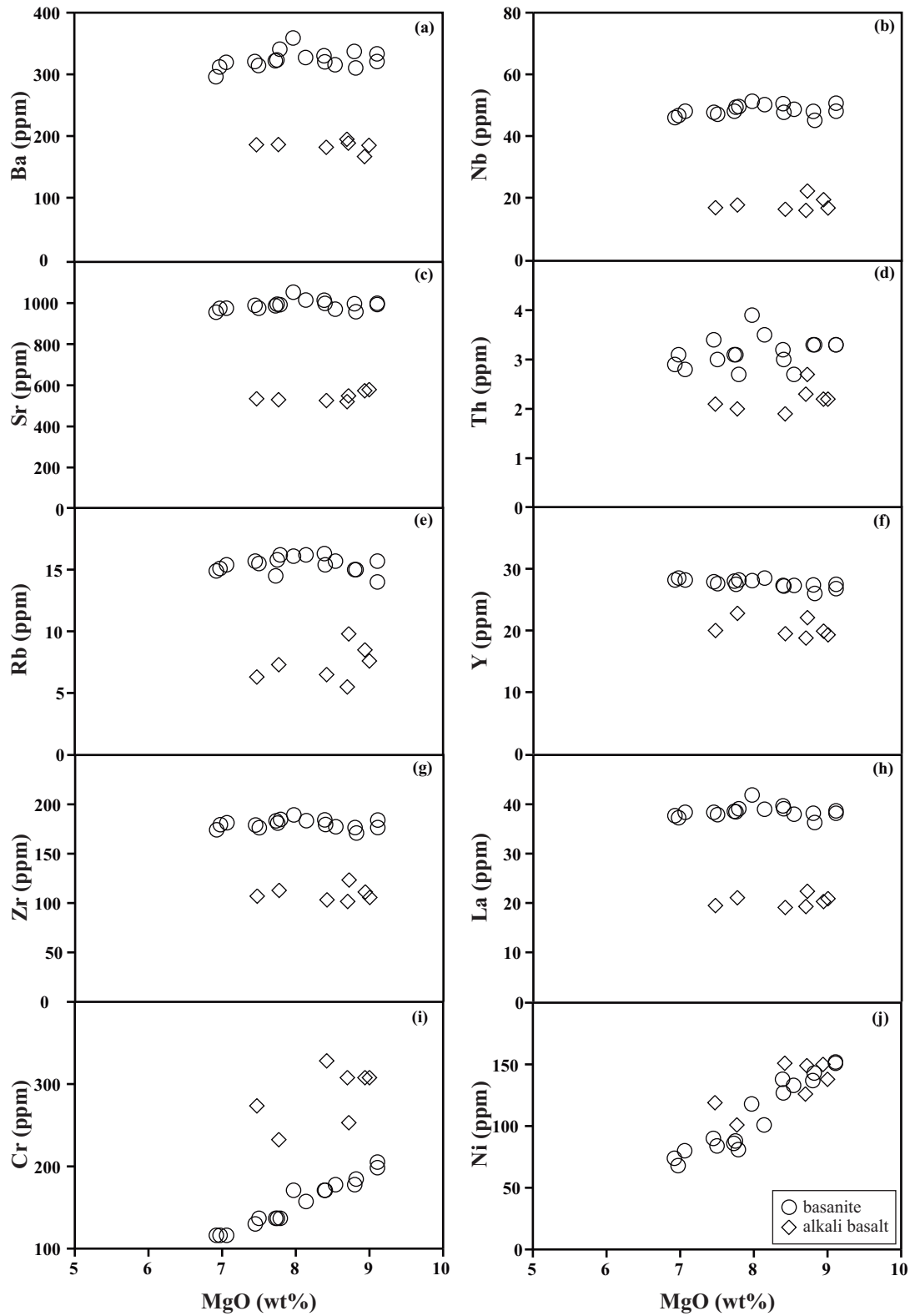
Figure 5. Trace element variation diagrams of alkali basalts and basanites from the Toprakkale volcanic unit.
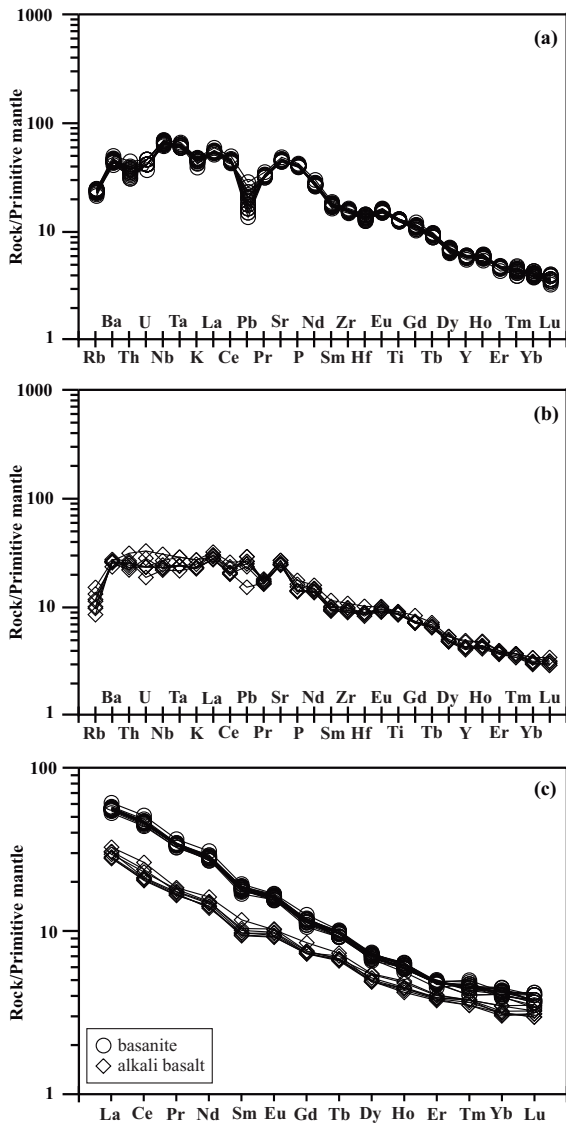
Figure 6. Primitive mantle normalized spider diagrams for alkali basalts and basanites from the Toprakkale volcanic unit (normalizing values are from Sun & McDonough 1989).

assimilation, fractional crystallization, degree of partial melting and source characteristics will be discussed below.

Crustal Assimilation

Determining the effects of crustal assimilation on the evolution of mantle derived melts during their passage to the surface is important because the melts pass through the crustal rocks. It influences the geochemistry of the melts, giving rise to elevated SiO_2, K_2O, Rb, Th, U, and Pb contents, low ratios of Nb/U, Ce/Pb and K/Nb, and positive spikes of K, Rb, and Pb on the normalized trace element patterns (Weaver & Tarney 1984).

On a primitive mantle normalized diagram the trace element patterns of the basanites show slight negative Th, U, K anomalies and a negative Pb anomaly (Figure 6a) relative to Ba, Nb (and Ta). Their Nb/La ratios vary from 1.22 to 1.28, indicating that the crustal assimilation process did not play any role in the basanite evolution. However, their depleted Sr isotopic ratios and elevated Nd isotope ratios do not indicate any crustal assimilation (Hoffmann *et al.*1986). The alkali basalts have a positive Pb anomaly except for one sample (Figure 6b). They display neither negative nor positive K, Nb, U and Ta anomalies (Figure 6b), but have lower ratios of Nb/U and Ce/Pb, and higher ratios of Ba/Nb, K/Nb and La/Nb compared to the basanites, implying that some crustal assimilation occurred (Table 2), although Nb/Ta ratios (16.3–18.5) are similar to mantle values (17.5±2.5 for mantle, Sun & McDunough 1989). The positive Pb anomaly and enriched Sr isotopic ratio also suggest that some crustal assimilation occurred during the evolution of the alkali basalts.

Fractional Crystallization

Crystal fractionation processes have a major role on the geochemical characteristics of melts. They result in large compositional ranges within the same suite and hence decreasing and/or increasing trends are seen on the binary diagrams.

Geochemical analyses of both the volcanic units show limited compositional ranges for both basanites and alkali basalts. Most of the major and trace elements show poor or no correlation with MgO as fractionation index (Figures 4 & 5). Nevertheless, some major (Fe_2O_3, Al_2O_3 and CaO) and compatible trace elements (Cr and Ni) can be correlated with MgO, indicating the presence of some crystal fractionation (Figures 4 & 5). The positive Fe_2O_3, Cr and Ni trends versus MgO (Figures 4e & 5i, j) show that olivine was a
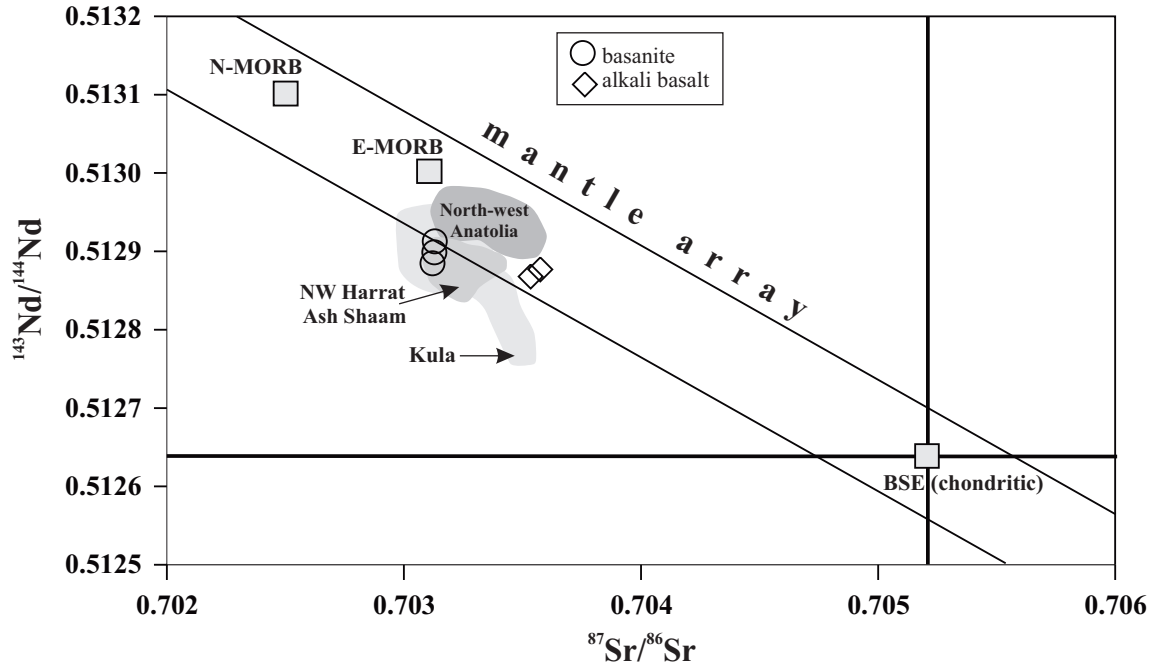
Figure 7. $^{87}Sr/^{86}Sr$ versus the $^{143}Nd/^{144}Nd$ isotope diagram showing the representative samples from the Toprakkale volcanic unit. MORB compositions are from Zindler & Hart (1986); BSE (bulk silicate earth) composition is from Hart *et al.* (1992). The fields for the Kula region (Alıcı *et al.* 2002), the Plio-Quaternary mafic volcanics in north-west Anatolia (Aldanmaz *et al.* 2006), and NW Harrat Ash Shaam, Israel (Weinstein *et al.* 2006) are shown.

Table 3. Sr and Nd isotope data for alkali basalts and basanites from the Toprakkale volcanic unit.

Sample	$^{87}Sr/^{86}Sr$	$^{143}Nd/^{144}Nd$	ε_{Nd}
Basanites			
10	0.703128	0.512899	5.091312
21	0.703120	0.512885	4.818215
24	0.703130	0.512913	5.364409
Alkali Basalts			
13	0.703575	0.512877	4.662159
14	0.703534	0.512868	4.486597

fractionating phase, as also indicated by petrographical features (Table 1). Negative correlation of CaO may indicate plagioclase fractionation (Figure 4g). Since the plagioclase only occurs late as a groundmass phase (Table 1),

plagioclase fractionation can be eliminated. Chemical evidence for the insignificance of plagioclase fractionation during magma evolution comes from the negative correlation between Al_2O_3 and MgO (Figure 4c) and the lack of relative depletion of Sr and Eu on the primitive mantle normalized trace and REE patterns (Figure 6a–c). Small positive Eu anomalies on REE patterns (Figure 6c) cannot also be explained by plagioclase fractionation. Positive Eu anomalies must have been inherited from the source and may reflect residual clinopyroxene, as suggested by Hanson (1980). These data imply that the crystal fractionation has limited or no effect on the evolution of these units. Therefore compositional differences between basanites and alkali basalts can be explained by varying degrees of partial melting of the same source, or source region characteristics which have different mineralogies.

Source Characteristics and Melting Depth

Certain element ratios are used to determine source region characteristics and partial melting depth. These characteristics are observed more clearly where Na/Ti and Sm/Yb ratios are compared to MgO content diagrams (Figure 8). CaO/Al_2O_3 ratio has a close relation with source region mineralogy whereas Na/Ti ratios act quite sensitively in response to melting pressure (Putirka 1999). Melts with a high CaO/Al_2O_3 ratio indicate a clinopyroxene-enriched source region (Herzberg & Zhang 1996; Hirose & Kushiro 1993). This characteristic also shows the existence of a residual garnet phase in the source region (Walter *et al.* 1995; Walter 1998). The alkali basalts and basanites have quite constant CaO/Al_2O_3 ratios suggesting that their source region mineralogy is quite similar (Figure 8a). Na/Ti ratios of melts decrease with increasing pressure because $Ca^{cpx}_{Na}/Ca_{Na}^{melt}$ increases with increased pressure while $D^{min/melt}_{Ti}$ remains constant or decreases (Langmuir *et al.* 1992; Blundy *et al.* 1995; Kinzler 1997; Walter 1998; Putirka 1999). The Na/Ti ratios of alkali basalts and basanites compared to MgO contents indicate that basanites have lower Na/Ti ratios than the alkali basalts (Figure 8b). This implies that the basanites derived from melts which occurred at higher pressures than that of the alkali olivine basalts.

Figure 8c plots Sm/Yb ratios against MgO. The basanites have higher Sm/Yb ratios than the alkali basalts. Differences among the Sm/Yb ratios of samples of both units may originate from mineralogies of the different source regions and/or removal of those minerals which have high values of D_{Yb} relate to D_{Sm}. An explanation for lower Sm/Yb ratios is related to removal of garnet from the residual phase during partial melting (Putirka 1999). At the beginning of melting, the amount of garnet is at highest level in the source and, therefore, $D_{Yb}^{solid/melt}$ ratio is also at highest level ($D_{Yb}^{garnet/melt}$ is high, Putirka 1999). As the melting progresses, the amount of garnet in the residual phase tends to decrease, and $D_{Yb}^{solid/melt}$ also decreases (Putirka 1999). Removal of the garnet from the source region causes the Sm/Yb ratio to increase and the Yb content of the melt to decrease. When lithosphere thickness exceeds 75 km, all melting occurs in garnet

stability field (Takahashi *et al.* 1993; Longhi 1995; Kinzler 1997; Walter 1998). In this case, transition of the source region garnet to melt can be estimated from the Sm/Yb ratio. The Sm/Yb ratio of the basanites is higher than the Sm/Yb ratio of the alkali basalts (Figure 8c). This characteristic shows that basanites are the products of melts which occurred in higher pressures (depths) than the alkali basalts.

One of the most important characteristics observed in primitive mantle normalized trace element patterns is the low observed values of Ba, Rb and K compared to Nb and Ta. This characteristic requires the existence of residual phases, such as phlogopite or amphibole, which contain elements such as K and Rb in the source region. Mineral/melt partition coefficients show that Ba, Rb and K are compatible in phlogopite (La Tourette *et al.* 1995; Chazot *et al.* 1996; Foley *et al.* 1996; Schmidt *et al.* 1999), but they show that Ba and K are only compatible in amphibole within the mantle (Chazot *et al.* 1996; Bottazzi *et al.* 1999; Tiepolo *et al.* 2000). The primitive mantle normalized spider and REE diagrams indicate that there was residual phlogopite and/or amphibole in the source region during the formation of the basanites and alkali basalts. If the phlogopite remains as residual phase during the melting of the source, profiles will be enriched in high field strength elements (HFSEs) and rare earth elements (REEs) in primitive mantle normalized trace element and rare earth element diagrams. When melting starts it excludes fusion of garnet and phlogopite as residual phases, but in the later stages of the melting these residual phases and other mantle phases will also partly melt (Foley 1992).

Primitive mantle normalized trace element patterns of the basanites are characterized by negative K-Rb and positive Nb-Ta anomalies resembling those of HIMU-OIB basalts (Weaver 1991, Figure 6a), while those of the alkali basalts do not show Nb-Ta enrichment (Figure 6b). The isotopic compositions of the basanites fall into the depleted quadrant of the conventional Sr-Nd isotopic space (Figure 7). Trace element ratios show that the basanites and alkali basalts plot in the OIB field (Figure 9a). A Ba/Nb - La/Nb diagram for the Toprakkale volcanic unit displays enrichments in highly mobile elements relative to immobile
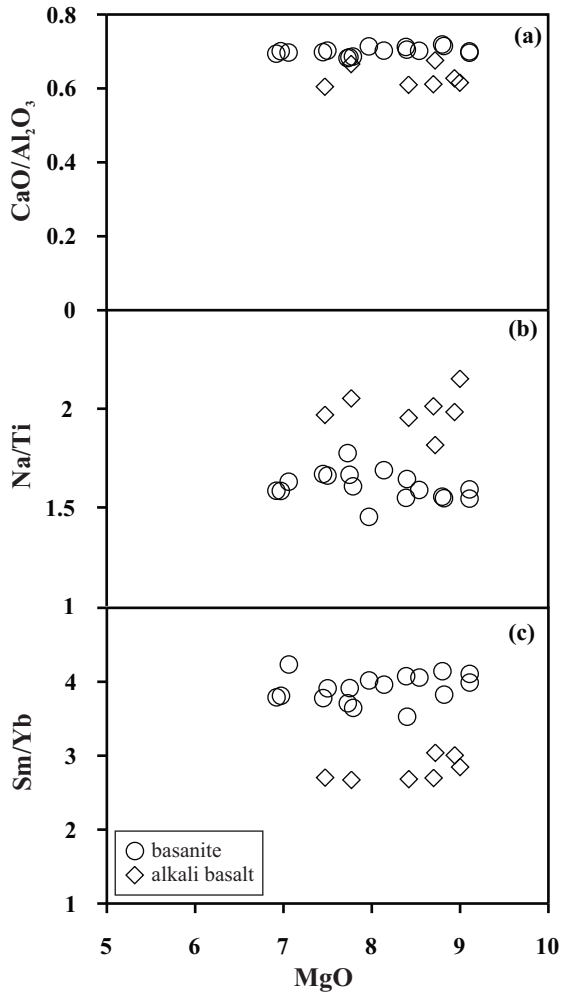
Figure 8. MgO - CaO/Al$_2$O$_3$ **(a)**; MgO - Na/Ti **(b)**; MgO - Sm/Yb **(c)** diagrams for alkali basalts and basanites from the Toprakkale volcanic unit.
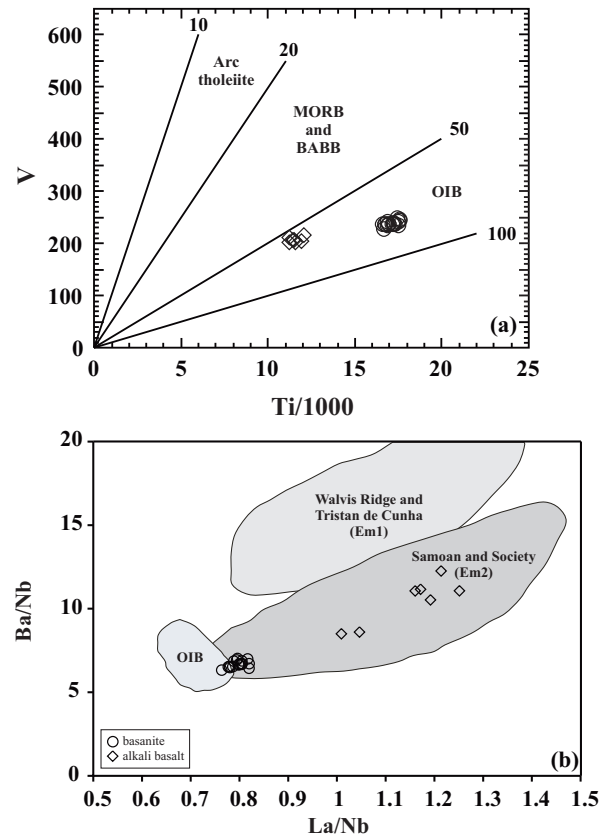

Figure 9. **(a)** V-Ti discrimination diagram for alkali basalts and basanites from the Toprakkale volcanic unit. Ranges of Ti/V ratios for MORB– mid-ocean ridge-basalt, BABB– backarc basin basalt, OIB– ocean island basalt from Shervais (1982). **(b)** Ba/Nb versus La/Nb diagram for alkali basalts and basanites from the Toprakkale volcanic unit. EM1– enriched mantle 1 (oceanic lithospheric mantle) EM2– enriched mantle 2 (subcontinenal lithospheric mantle). Oceanic basalts fields from Sun & McDonough 1989; end-members from Weaver 1991.

elements, implying that the basalts could have originated from an enriched mantle source (Figure 9b). Both the basanites and alkali basalts are enriched in high field strength elements such as Ti (Table 1), and the high Ti contents are incompatible with the melting of spinel and garnet-peridotite. The average Ti content of subcontinental lithospheric mantle obtained from peridotite xenoliths does not exceed 0.21% (Griffin *et al.* 1999). Experimental studies display high TiO$_2$ content in low melting fractions (Mysen & Kushiro 1977; Jaques & Green 1980; Falloon & Green 1987; Baker & Stolper 1994; Falloon *et al.* 1997; Kinzler 1997; Kogiso *et al.* 1998;

Robinson *et al.* 1998). However, in experimental studies on peridotites containing 0.17% TiO$_2$, the melts had a maximum 1.3% TiO$_2$ content, even where the melt proportion was lower than 1% (Robinson *et al.* 1998). Taking this into account, a source enriched in Ti and other high field strength elements is thus required for the formation of the basanites and alkali basalts. Clinopyroxenites, websterites and amphibolites are Ti-rich: they contain higher TiO$_2$, Al$_2$O$_3$ and incompatible elements than harzburgites and lherzolites. These

rock types also contain clinopyroxene, kaersutitic amphibole and/or phlogopite which are Ti-rich, and apatite, rutile and ilmenite as accessory minerals (Foley 1992; Witt-Eickschen & Harte 1994; McPherson *et al.* 1996; Woodland *et al.* 1996; Kopylova *et al.* 1999; Ho *et al.* 2000b; Downes 2001). Using these arguments with regard to the trace element data of both the basanites and the alkali basalts, the source region is unlikely to be purely garnet or spinel-peridotitic material. The higher Ti content requires the peridotitic source region to contain clinopyroxene and/or phlogopite/amphibole (Foley 1992). Therefore the geochemical and isotopic characteristics of the basanites and alkali basalts suggest that the source region was enriched in LILE and LREE with a depleted isotopic signature. The enrichment process was possibly due to subduction-related metasomatism that may be consequence of the earlier subduction events, which formed the pyroxenitic veins in the mantle wedge (Foley 1992).

Partial Melting

The alkali basalts and basanites of the Toprakkale volcanic unit have similar trace element and REE patterns on primitive mantle normalized diagrams (Figure 6). This situation requires that the melts were formed from the same parent material with varying degrees of partial melting. Determination of the geochemical characteristics of mantle-derived basaltic magmas, the nature of the melting process, the degree of partial melting, the magma extraction, aggregation processes, values for the partition coefficient between mantle minerals and basaltic magma all allow different models to be made for the chemical, mineralogical and isotopic characteristics of the mantle source (Zou & Zindler 1996). The most important problem is the assumption of the proportion of partial melting forming the basaltic melt. For instance, the degree of partial melting in the batch melting model can only be estimated from trace element concentration in the magma by assuming concentration levels in the source (Zou & Zindler 1996). This can lead to significant error in the estimated degree of partial melting. For instance, heavy rare earth elements (HREE) concentrations in the basalts can reach 1–7 times chondritic values (Frey 1969; Kay & Gast 1973; Loubet *et al.* 1975;

Clague & Frey 1982). Therefore, to minimize the errors on the calculated source region concentrations and the degree of partial melting, actual concentrations from the basalts without any assumptions about source region concentrations should be used (Zou & Zindler 1996). There are two methods for calculating the approximate proportion of partial melting. The first of these methods is the concentration ratio (CR method, Maaloe 1994) based on the incompatible trace element ratio of two different magmas considering to have been derived from the same source, and the second is source ratio, which is based on the estimation of concentration ratios in the source (SR method, Treuil & Joron 1975; Minster & Allegre 1978; Hoffmann & Feigenson 1983; Cebriá & Lopez-Ruiz 1995). Both methods have limitations and give some calculations with errors. Therefore, dynamic melting calculations proposed by Langmuir *et al.* (1977) and formulated by McKenzie (1985) and Maaloe & Johnston (1986) are preferred. Using the actual concentrations in the melts is very useful in calculating the degree of partial melting and source region concentrations (Ribe 1988; Hemond *et al.* 1994).

In the Toprakkale region, the alkali basaltic and basanitic samples occur together. Since the isotopic characteristics of these rocks display some similarities, dynamic melting modelling was made using concentration ratios (Figure 7). Dynamic melting has been calculated by assuming that both melts derived from same source region and source concentrations have been found fitting the melt proportions obtained from dynamic melting modelling. Samples with lowest SiO_2 contents for both rock types have been chosen as a primitive melts (sample 21 for basanites and sample 13 for alkali basalts). The alkali basalts were formed with 9.19% partial melting whereas the basanites were formed with 4.58% partial melting (Table 4). The calculated source region concentrations imply that the enriched source region characteristics were as in primitive mantle concentrations (Table 4).

Figure 10a displays non-modal batch melting curves of garnet and spinel-peridotite sources and La/Yb$_N$-Dy/Yb$_N$ data from the alkali basalts and basanites. The La/Yb ratio decreases with the increase in melting proportion. Variations in the

Table 4. Calculation of partial melting degrees and mantle source compositions for alkali basalts and basanites of the Toprakkale volcanic unit. Partial melting degrees have been calculated using dynamic modelling of Zou & Zindler (1996). D– bulk distribution coefficients (mineral melt partition coefficients from McKenzie & O'Nions 1991, and mantle mode from Kinzler 1997); Q– enrichment concentration ratio; Co– source concentration; ϕ_1– partial melting degree for alkali basalts; ϕ_2– partial melting degree for basanites.

Element	D	Alkali Basalt	Basanite	Q	ϕ_1 (%)	ϕ_2 (%)	Co
Nb	0.001945	22.2	50.70	2.28			
La	0.00664	22.4	38.70	1.73	4.29	5.24	1.87
Ce	0.0119	46.7	82.50	1.77	2.61	5.7	4.22
Nd	0.0277	21.9	36.50	1.66	4.6	9.63	2.3
Sm	0.0512	5.2	8.30	1.59	5.43	11.42	0.61
Eu	0.0598	1.71	2.69	1.57	6.31	13.38	0.23
Gd	0.0925	5.06	6.74	1.33	4.21	8.81	0.62
Tb	0.115	0.79	1.00	1.26	4.12	8.64	0.11
Dy	0.1384	4.04	5.12	1.27	5.11	10.72	0.63
Average					9.19	4.58	

Dy/Yb ratio reflect the existence of garnet in the source region. For the source region concentrations, primitive mantle values of Sun & McDonough (1989) have been used. Partial melting of both spinel and garnet peridotite in varying proportions cannot explain the La/Yb$_N$ and Dy/Yb$_N$ variation in alkali basalts and basanites in Figure 10a. However, non-modal batch melting calculations with source region concentration obtained from dynamic melting indicate that the basanites and alkali basalts could have formed by partial melting of such an enriched source although they plot on somewhat higher proportions on the partial melting trajectory (Figure 10b).

Geodynamic Implications

Complex plate tectonic movements between the Arabian and African plates and the Eurasian plate along the Bitlis Suture Zone and the Hellenic Arc have controlled the neotectonic development of Turkey (Şengör & Yılmaz 1981; Şengör *et al.* 1985; Dewey *et al.* 1986; Taymaz *et al.* 1990). The major tectonic alignments of Turkey, the East (sinistral) and North Anatolian (dextral) strike-slip fault zones, formed as a result of the compressional regime between the Arabian and the Eurasian plates (along the Bitlis Suture Zone) which also caused crustal uplift and shortening of the Eastern Anatolia region (Dewey *et al.* 1986; Oral *et al.* 1995). Recent continuous northward movements of the African and Arabian plates give rise to westward movement of the Anatolian plate (Şengör & Yılmaz 1981; Yılmaz *et al.* 1988; Karig & Kozlu 1990; Westaway & Arger 1996; Arger *et al.* 2000). The Hellenic and Cyprus arcs, with related subduction, have been evolved as a result of the northward movement of the African Plate in the Eastern Mediterranean region (McKenzie 1972; Barka & Reilinger 1997).

Evolutionary studies (mainly general geology, structural geology, basin evolution) of the southern Turkey and Eastern Mediterranean regions revealed a transtensional tectonic regime dominance since the Late Pliocene (Parlak *et al.* 2000). This tectonic regime produced the intra-continental basaltic volcanism along the main structural alignments such as the left-lateral strike-slip Yumurtalık fault zone (Figure 1; Kozlu 1987; Kelling *et al.* 1987; Karig & Kozlu 1990; Parlak *et al.* 1997, 1998). Transtensional movements at the boundary between the African and Anatolian plates (White & McKenzie 1989) gave rise to decompressional melting beneath the plates of mantle material that had been subjected to subduction-related metasomatism during earlier subduction events. Consequently, this evidence suggests that magma evolution resulting from decompression in a transtensional extensional regime, and movement on the sinistral Yumurtalık Fault opened a way for this magma to rise to the surface.
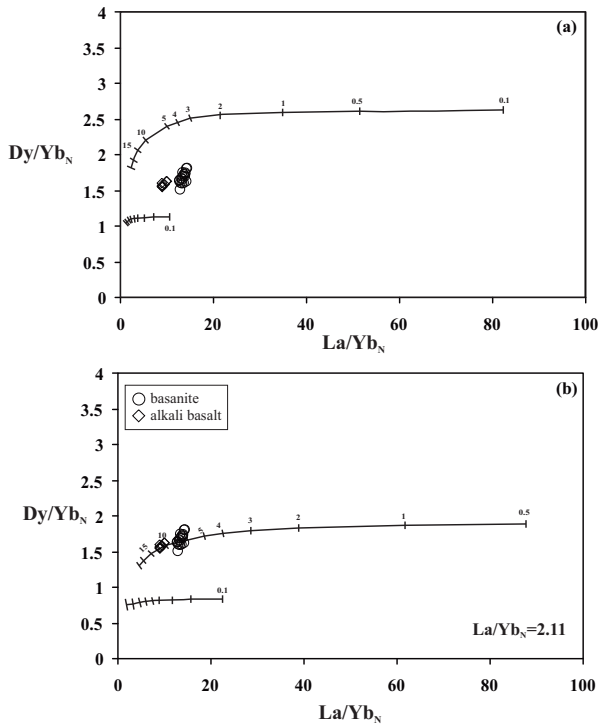
Figure 10. La/Yb$_N$ - Dy/Yb$_N$ diagrams for alkali basalts and basanites from the Toprakkale volcanic unit. Non-modal batch melting curves of garnet and spinel-peridotite sources with primitive mantle values are from Sun & McDonough 1989) as source concentrations **(a)**; non-modal batch melting curves using source concentrations calculated from dynamic melting results **(b)**. Normalizing values are from Sun & McDonough (1989); spinel-peridotite source and melt mode values are from Kinzler (1997); garnet-peridotite source and melt mode values are from Walter (1998); mineral/melt partition coefficients are from McKenzie & O'Nions (1991); Nielsen *et al.* (1992); Hart & Dunn (1993); Dunn & Sen (1994); le Roex *et al.* (1996).

Concluding Remarks

1. The volcanic rocks of Toprakkale in the Yumurtalık fault zone consist of alkali basalts and basanites.

2. These rocks display similar geochemical features, but are characterized by different enrichments in LILE and LREE, indicating that the melts were derived from the same source with different proportions of partial melting.

3. Sr, and Nd isotope compositions of the alkali basalts show that they originated from an isotopically depleted and chemically enriched mantle source.

4. Negative K anomalies seen in the basanites imply the presence of a K-bearing phase or phases in the mantle source, which buffer this element.

5. Higher TiO$_2$ contents of both rock types show that the melts did not originate purely from peridotitic material, but were derived from a source region with TiO$_2$ rich material such as pyroxenites.

6. Overall geochemical characteristics suggest the presence of subduction-related metasomatism.

7. The alkali basalts and basanites were formed with 9.19% and 4.58% partial melting proportions based on the dynamic melting calculation of Zou & Zindler (1996).

8. Melts originating from an enriched source region occurred due to decompressional melting as a result of transtensional tectonics.

Acknowledgments

References

Aksu, A.E., Calon, T.J., Hall, J., Mansfield, S. & Yaşar, D. 2005. The Cilicia-Adana basin complex, Eastern Mediterranean: Neogene evolution of an active fore-arc basin in an obliquely convergent margin. *Marine Geology* **221**, 121–159.

Albora, A.M., Sayın, N. & Uçan, O.N. 2006. Evaluation of tectonic structure of İskenderun Basin (Turkey) using steerable filters. *Marine Geophysic Research* **27**, 225–239.

ALDANMAZ, E., KÖPRÜBAŞI, N., GÜRER, O.F., KAYMAKCI, N. & GOURGAUD, A. 2006. Geochemical constraints on the Cenozoic, OIB-type alkaline volcanic rocks of NW Turkey: implications for mantle sources and melting processes. *Lithos* **86**, 50–76.

ALICI, P., TEMEL, A., GOURGAUD, A. 2002. Pb–Nd–Sr isotope and trace element geochemistry of Quaternary extension related alkaline volcanism: a case study of Kula region (western Anatolia, Turkey). *Journal of Volcanology and Geothermal Research* **115**, 487–510.

ALICI, P., TEMEL, A., GOURGAUD, A., VIDAL, P. & GÜNDOĞDU, M.N. 2001. Quaternary tholeiitic to alkaline volcanism in the Karasu valley, Dead Sea rift zone, southeast Turkey: Sr-Nd-Pb-O isotopic and trace-element approaches to crust-mantle interaction. *International Geology Review* **43**, 120–38.

ANDERSON, D.L. 1994. Lithosphere and flood basalts. *Nature* **367**, 226–226.

ARGER, J., MITCHELL, J. & WESTAWAY, R. 2000. Neogene and Quaternary volcanism of south-eastern Turkey. *In:* BOZKURT, E., WINCHESTER, J.A. & PIPER, J.D.A. (eds), *Tectonics and Magmatism of Turkey and the Surrounding Area.* Geological Society, London, Special Publications **173**, 459–487.

BAKER, M.B. & STOLPER, E.M. 1994. Determining the composition of high-pressure mantle melts using diamond aggregates. *Geochimica et Cosmochimica Acta* **58**, 2811–2827.

BARKA, A. & REILINGER, R. 1997. Active tectonics of Eastern Mediterranean region: deduced from GPS, neotectonic and seismicity data. *Annali DiGeofisica* **X2(3)**, 587–610.

BİLGİN, A.Z. & ERCAN, T. 1981. Petrology of the Quaternary basalts of Ceyhan-Osmaniye area. *Bulletin of Geological Society of Turkey* **24**, 21–30.

BLUNDY, J.D., FALLOON, T.J., WOOD, B.J. & DALTON, J.A. 1995. Sodium partitioning between clinopyroxene and silicate melts. *Journal of Geophysic Reaserchs* **100(B8)**, 15,501–15,515.

BOTTAZZI, P., TIEPOLO, M., VANNUCCI, R., ZANETTI, A., BRUMM, R., FOLEY, S.F. & OBERTI, R. 1999. Distinct site preferences for heavy and light REE in amphibole and the prediction of Amph/LDREE. *Contributions to Mineralogy and Petrology* **137**, 36–45.

CAMPBELL, I.H. & GRIFFITHS, R.W. 1990. Implications of mantle plume structure for the evolution of flood basalts. *Earth and Planetary Science Letters* **90**, 79–93.

ÇAPAN, U.Z., VIDAL, P.H. & CANTAGREL, J.M. 1987. K-Ar, Nd, Sr and Pb isotopic study of Quaternary volcanism in Karasu valley (Hatay), N-end of Dead Sea rift zone in SE-Turkey. *Yerbilimleri* **14**, 165–178.

CEBRIÁ, J.M. & LÓPEZ-RUIZ, J. 1995. Alkali basalts and leucitites in an extensional intracontinental plate setting: the Late Cenozoic Calatrava Volcanic Province (Central Spain). *Lithos* **35**, 27–46.

CHAZOT, G., MENZIES, M. & HARTE, B. 1996. Determination of partition coefficients between apatite, clinopyroxene, amphibole and melt in natural spinel lherzolites from Yemen: implications for wet melting of the lithosphere mantle. *Geochimica et Cosmochimica Acta* **60**, 423–437.

CHOROWICZ, J., LUXEY, P., LYBERIS, N., CARVALHO, J., PARROT, J.F., YÜRÜR, T. & GÜNDOĞDU, M.N. 1994. The Maraş triple junction, southern Turkey, based on digital elevation model and satel-lite imagery interpretation. *Journal of Geophysic Reaserch* **99 (B10)**, 20225–20242.

CLAGUE, D.A. & FREY, F.A. 1982. Petrology and trace element geochemistry of the Honolulu volcanism and implications for the oceanic mantle below Hawaii. *Journal of Petrology* **23**, 447–504.

DEWEY, J.F., HEMPTON, M.R., KIDD, W.S.F., ŞAROĞLU, F. & ŞENGÖR, A.M.C. 1986. Shortening of continental lithosphere: the neotectonics of Eastern Anatolia - a young collision zone: *In:* COWARD, M.P. & RIES, A.C (eds), *Collision Tectonics.* Geological Society, London, Special Publications **19**, 3–36.

DİLEK, Y., THY, P., HACKER, B. & GRUNDVIG, S. 1999. Structure and Petrology of Tauride ophiolites and mafic dike intrusions (Turkey): implications for the Neotethyan Ocean. *GSA Bulletin* **111**, 1192–1216.

DOWNES, H. 2001. Formation and modification of the shallow sub-continental lithospheric mantle: a review of geochemical evidence from ultramafic xenolith suites and tecto-nically emplaced ultramafic massifs of Western and Central Europe. *Journal of Petrology* **42**, 233–250.

DUNN, T. & SEN, C. 1994. Mineral/matrix partition coefficients for orthopyroxene, plagioclase, and olivine in basaltic to andesitic systems: a combined analytical and experimental study. *Geochimica et Cosmochimica Acta* **58**, 717–733.

FALLOON, T.J. & GREEN, D.H. 1987. Anhydrous partial melting of MORB pyrolite and other peridotite compositions at 10 kbar and implications for the origin of primitive MORB glasses. *Minerology and Petrology* **37**, 181–219.

FALLOON, T.J., GREEN, D.H., O'NEILL, H.S.C. & HIBBERSON, W.O. 1997. Experimental tests of low degree peridotite partial melt compositions: implications for the nature of anhydrous near-solidus peridotite melts at 1 GPa. *Earth and Planetary Science Letters* **152**, 149–162.

FOLEY, J.A., PRENTICE, I.C., RAMANKUTTY, N., LEVIS, S., POLLARD, D., SITCH, S. & HAXELTINE, A. 1996. An integrated biosphere model of land surface processes, terrestrial carbon balance, and vegetation dynamics. *Global Biogeochemical Cycles* **10**, 603–628.

FOLEY, S. 1992. Vein-plus-wall-rock melting mechanisms in the lithosphere and the origin of potassic alkaline magmas. *Lithos* **28**, 435–453.

FREY, F.A. 1996. Rare earth abundances in a high-temperature peridotite intrusion. *Geochimica et Cosmochimica Acta* **33**, 1429–1447.

GRIFFIN, W.L., O'REILLY, S.Y. & RYAN, C.G. 1999. The composition and origin of subcontinental lithospheric mantle, *In:* FEI, Y., BERTKA, C.M. & MYSEN, B.O. (eds), *Mantle Petrology: Field Observations and High-pressure Experimentation: A Tribute to Francis R. (Joe) Boyd.* Houston, Texas, The Geochemical Society, Special Publications **6**, 13–43..

HANSON, G.N. 1980. Rare earth elements in petrogenetic studies of igneous rock systems. *Annual Review of Earth and Planetary Sciences* **9**, 371–406.

HART, S.R. & DUNN, T. 1993. Experimental cpxlmelt partitioning of 24 elements. *Contributions to Mineralogy and Petrology* **1**, 1–8.

HART, S.R., HAURI, E.H., OSCHMANN, L.A., WHITEHEAD, J.A., 1992. Mantle plumes and entrainment: isotopic evidence. *Science* **256**, 517–520.

HEMOND, C., HOFMANN, A.W., HEUSSER, G., CONDOMÍNES, M., RACZEK, I. & RHODES, J.M. 1994. U-Th-Ra systematics in Kilauea and Mauna-Loa basalts, Hawaii. *Chemical Geology* **116**, 163–180.

HERZBERG, C. & ZHANG, J. 1996. Melting experiments on anhydrous peridotite KLB-1: compositions of magmas in the upper mantle and transition zone. *Journal of Geophysical Research* **101**, 8271–8295.

HIROSE, K. & KUSHIRO, I. 1993. Partial melting of dry peridotites at high pressures: determination of compositions of melts segregated from peridotite using aggregates of diamond. *Earth and Planetary Science Letters* **114**, 477–489.

HO, K.S., CHEN, J.C., SMITH, A.D. & JUANG, W.S. 2000. Petrogenesis of two groups of pyroxenite from Tungchihsu, Penghu Islands, Taiwan Strait: implications for mantle metasomatism beneath SE China. *Chemical Geol*ogy **167**, 355–372.

HOFFMANN, A.W. & FEIGENSON, M.D. 1983. Case studies on the origin of basalt: 1. Theory and reassessment of Grenada basalts. *Contributions to Mineralogy and Petrology* **84**, 382–389.

HOFFMANN, A.W., JOCHUM, K.P., SEUFERT, M. & WHITE, M.W. 1986. Nb and Pb in oceanic basalts: new constraints on mantle evolution. *Earth and Planetary Science Letters* **79**, 33–45.

IRVINE, T.N. & BARAGAR, W.R.A. 1971. A guide to the chemical classification of the common volcanic rocks: *Canadian Journal of Earth Sciences* **8**, 523–548.

JAQUES, A.L. & GREEN, D.H. 1980. Anhydrous melting of peridotite at 0–15 kb pressure and the genesis of tholeiitic basalts. *Contributions to Mineralogy and Petrology* **73**, 287–310.

KARIG, D.E. & KOZLU, H. 1990. Late Palaeogene–Neogene evolution of the triple junction region near Maraş, south-central Turkey. *Journal of the Geological Society, London* **147**, 1023–1034.

KAY, R. & GAST, P.W. 1973. The rare earth element content and origin of alkali-rich basalts. *Journal of Geology* **81**, 653–682.

KELLING, G., GÖKÇEN, S.L., FLOYD, P.A. & GÖKÇEN, N. 1987. Neogene tectonics and plate convergence in the eastern Mediterranean: New data from southern Turkey. *Geology* **15**, 425–429.

KING, S.D. & ANDERSON, D.L. 1995. An alternative mechanism of flood basalt formation. *Earth and Planetary Science Letters* **136**, 269–279.

KING, S.D. & ANDERSON, D.L. 1998. Edge-driven convection. *Earth and Planetary Science Letters* **160**, 289–96.

KINZLER, R.J. 1997. Melting of mantle peridotite at pressures approaching the spinel to garnet transition: application to midocean ridge basalt petrogenesis. *Journal of Geophysical Research* **102**, 853–874.

KOGISO, T., HIROSE, K. & TAKAHASHI, E. 1998. Melting experiments on homogeneous mixtures of peridotite and basalt: applications to the genesis of ocean island basalts. *Earth and Planetary Science Letters* **162**, 45–61.

KOPYLOVA, M.G., RUSSELL, J.K. & COOKENBOO, H. 1999. Petrology of peridotite and pyroxenite xenoliths from the Jericho kimberlite: implications for the thermal state of the mantle beneath the Slave craton, Northern Canada. *Journal of Petrology* **40**, 79–104.

KOZLU, H. 1987. Misis-Andırın dolaylarının stratigrafisi ve yapısal evrimi [Stratigraphy and structural evolution of Misis-Andırın region]. *Türkiye 7. Petrol Kongresi*, *Proceedings*, 104–116 [in Turkish with English abstract].

LA TOURETTE, T., HERVIG, R.L. & HOLLOWAY, J.R. 1995. Trace element partitioning between amphibole, phlogopite, and basanite melt. *Earth and Planetary Science Letters* **135**, 13–30.

LANGMUIR, C.H., BENDER, J.F., BENCE, A.E., HANSON, G.N. & TAYLOR, S.R. 1977. Petrogenesis of basalts from the Famous area: mid-Atlantic Ridge. *Earth and Planetary Science Letters* **36**, 133–156.

LANGMUIR, C.H., KLEIN, E.M. & PLANK, T. 1992. Petrological systematics of mid-ocean ridge basalts: Constraints on melt generation beneath ocean ridges. *In:* PHIPPS MORGAN, J., BLACKMAN, D.K. & SINTON, J.M. (eds), *Mantle Flow and Melt Generation at Mid-Ocean Ridges.* American Geophysical Union, Geophysical Monographies **71**, 183–280.

LE ROEX, A.P., FREY, F.A. & RICHARDSON, S.H. 1996. Petrogenesis of lavas from the AMAR Valley and Narrowgate region of the FAMOUS Valley, 36_–37_N on the Mid-Atlantic Ridge. *Contributions to Mineralogy and Petrology* **124**, 167–184.

LE MAITRE, R. W., BATEMAN, P., DUDEK, A., KELLER, J., LAMEYRE, LE BAS, M.J., SABINE, P.A., SCHMID, R., SORENSEN, H., STREICKESEN, A., WOOLLEY, A.R. & ZANETTIN, B. 1989. *A Classification of Igneous Rocks and Glossary of Terms.* Oxford, Blackwell.

LONGHI, J. 1995. Liquidus equilibria of some primary lunar and terrestrial melts in the garnet stability field. *Geochimica et Cosmochimica Acta* **59**, 2375–2386.

LOUBET, M., SHIMIZU, N. and ALLE`GRE, C. 1975. Rare earth elements in Alpine peridotites. *Contributions to Mineralogy and Petrology* **53**, 1–12.

MAALOE, S. 1994. Estimation of the degree of partial melting using concentration ratios. *Geochimica et Cosmochimica Acta* **58**, 2519–2525.

MAALOE, S. & JOHNSTON, A.D. 1986. Geochemical aspects of some accumulation models for primary magmas. *Contributions to Mineralogy and Petrology* **93**, 449–458.

MCKENZIE, D.P. 1972. Active tectonics of the Mediterranean region. *Geophysical Journal of the Royal Astronomical Society* **30**, 109–185.

MCKENZIE, D. 1985. ^{230}Th-^{238}U disequilibrium and melting processes beneath ridge axes. *Earth and Planetary Science Letters* **72**, 149–157.

MCKENZIE, D.P. & O'NIONS, R.K. 1991. Partial melt distribution from inversion of rare earth element concentrations. *Journal of Petrology* **32**, 1021– 1991.

MCPHERSON, C.E., HOROWITZ, R., WOODCOCK, C.L., JIANG, C. & ZARET, K.S. 1996. Nucleosome positioning properties of the albumin transcriptional enhancer. *Nucleic Acids Research* **24,** 397–404.

MINSTER, J.F. & ALLEGRE, C.J. 1978. Systematic use of trace elements in igneous processes. III: Inverse problem of batch partial melting in volcanic suites. *Contributions to Mineralogy and Petrology* **68**, 37–52.

MYSEN, B.O. & KUSHIRO, I. 1977. Compositional variations of coexisting phases with degree of melting of peridotite in the upper mantle. *American Mineralogist* **62**, 843-865.

NIELSEN, R.L., GALLAHAN, W.E. & NEWBERGER, F. 1992. Experimentally determined mineral-melt partition coefficients for Sc, Y and REE for olivine, orthopyroxene, pigeonite, magnetite and ilmenite. *Contributions to Mineralogy and Petrology* **110**, 488–499.

NUR, A. & BEN-AVRAHAM, Z. 1978. Speculation on mountain building and the lost Pacifica continent**.** *Journal of Physics of the Earth* **26**, S21–S37.

ORAL, M.B., KING, R. W., BARKA, A. A., KINIK, L. & LENG, O. 1995. Global Positioning system offers evidence of plate motions in Eastern Mediterranean. *EOS. AGU.* **76**, 2, 9–11.

PARLAK, O., DELALOYE, M., KOZLU, H. & FONTIGNIE, D. 2000. Trace element and Sr-Nd isotope geochemistry of the alkali basalts observed along the Yumurtalık Fault (Adana) in southern Turkey. *Yerbilimleri* **22**, 137–148.

PARLAK, O., KOP, A., ÜNLÜGENÇ, U.C. & DEMİRKOL, C. 1998. Geochemistry and geochronology of basaltic rocks in the Karasu graben around Kırıkhan (Hatay), Southern Turkey. *Turkish Journal of Earth Sciences* **7**, 53–61.

PARLAK, O., KOZLU, H., DEMİRKOL, C. & DELALOYE, M. 1997. Intracontinental Plio-Quaternary volcanism along the African-Anatolian plate boundary, southern Turkey. *Ofioliti* **22**, 111–117.

PERİNÇEK, D. & ÇEMEN, İ. 1990. The Structural Relationship between the East Anatolian and Dead Sea Fault Zones in Southeastern Turkey. *Tectonophysics* **172**, 331–340.

POLAT, A., KERRICH, R. & CASEY, J.F. 1997. Geochemistry of Quaternary basalts erupted along the East Anatolian and Dead Sea fault zones of Southern Turkey: implications for mantle sources. *Lithos* **40**, 55–68.

PUTIRKA, K. 1999. Melting depths and mantle heterogeneity beneath Hawaii and the East Pacific Rise: constraints from Na/Ti and rare earth element ratios. *Journal of Geophysical Research* **104**, 2817–2829.

RIBE, N.M. 1988. Earth planet. *Earth and Planetary Science Letters* **88**, 37–46.

RICHARDS, M.A., DUNCAN, R.A. & COURTILLOT, V.E. 1989. Flood basalts and hot-spot tracks: plume heads and tails. *Science* **246**, 103–107.

ROBERTSON, A.H.F., ÜNLÜGENÇ, U., İNAN, N. & TASLI, K. 2004. The Misis-Andırın Complex: a Tethyan melange related to Mid-Tertiary subduction and diachronous continental collision in Southern Turkey. *Journal of Asian Earth Sciences* **2**, 413–453.

ROBINSON, J.A.C., WOOD, B.J. & BLUNDY, J.D. 1998. The beginning of melting of fertile and depleted peridotite at 1.5 GPa. *Earth and Planetary Science Letters* **155**, 97–111.

ROJAY, B., HEIMANN, A. & TOPRAK, V. 2001. Neotectonic and volcanic characteristics of the Karasu fault zone (Anatolia, Turkey): the transition zone between the Dead Sea transform and the East Anatolian fault zone. *Geodinamica Acta* **14**, 197–212.

SCHMIDT, K.H., BOTAZZI, P., VANUCCI, R. & MENGEL, K. 1999. Trace element partitioning between phlogopite, clinopyroxene and leucite lamproite melt. *Earth and Planetary Science Letters* **168**, 287–299.

SHAW, J.E., BAKER, J.A., MENZIES, M.A., THIRLWALL, M.F. & IBRAHIM, K.M. 2003, Petrogenesis of the largest intraplate volcanic field on the Arabian plate (Jordan): a mixed lithosphere–asthenosphere source activated by lithospheric extension. *Journal of Petrology* **44**, 1657–79.

SHERVAIS, J.W. 1982. Ti-V plots and the petrogenesis of modern and ophiolitic lavas. *Earth and Planetary Science Letters* **59**, 101–118.

SHIMIZU, N. & KUSHIRO, I. 1975. Partitioning of rare-earth elements between garnet and liquid at high-pressures – preliminary experiments. *Geophysical Research Letters* **2**, 413–416.

STEIN, M. & HOFMANN, A.W. 1992. Fossil plume head beneath the Arabian lithosphere? *Earth and Planetary Science Letters* **114**, 193–209.

STEIN, M., NAVON, O. & KESSEL, R. 1997. Chromatographic metasomatism of the Arabian-Nubian lithosphere. *Earth and Planetary Science Letters* **152**, 75–91.

SUN, S.S. & MCDONOUGH, W.F. 1989. Chemical and isotopic systematics of oceanic basalts: implication for mantle composition and processes. *In:* SAUNDERS, A.D. & NORRY, M.J. (eds), *Magmatism in the Ocean Basins.* Geological Society, London, Special Publications **42**, 313–345.

ŞENGÖR, A.M.C., GÖRÜR, N. & ŞAROĞLU, F. 1985. Strike-slip faulting and related basin formation in zones of tectonic escape: Turkey as a case study. *In*: BIDDLE, K.T. & CHRISTIE-BLICK, N. (eds), *Strike-slip Deformation, Basin Formation, and Sedimentation.* Society of Economic Paleontologists and Mineralogists Special Publications **37**, 227–264.

ŞENGÖR, A.M.C. & YILMAZ, Y. 1981. Tethyan evolution of Turkey: a plate tectonic approach. *Tectonophysics* **75**, 181–241.

TAKAHASHI, E., SHIMAZAKI, T., TSUZAKI, Y. & YOSHIDA, H. 1993. Melting study of a peridotite KLB-1 to 6.5 GPa, and the origin of basaltic magmas. *Philosophical Transactions of Royal Society, London, Serie A 342*, 105–120.

TATAR, O., PIPER, J.D.A., GÜRSOY, H., HEIMANN, A. & KOÇBULUT, F. 2004. Neotectonic deformation in the transition zone between the Dead Sea Transform and the East Anatolian Fault Zone, Southern Turkey: a palaeomagnetic study of the Karasu rift volcanism. *Tectonophysics* **385**, 17–43.

TAYMAZ, T., JACKSON, J. & WESTAWAY, R. 1990. Earthquake mechanisms in the Hellenic Trench near Crete. *Geophysical Journal International* **102**, 695–731.

TIEPOLO, M., VANNUCCI, R., OBERTI, R., FOLEY, S., BOTTAZZI, P. & ZANETTI, A. 2000. Nb and Ta incorporation and fractionation intitanian pargasite and kaersutite: crystal-chemical constraints and implications for natural systems. *Earth and Planetary Science Letters* **176**, 185–201.

TOLUN, N. & PAMİR, H.N. 1975. *Explanatory Booklet Accompanying the Hatay Sheet of the Geological Map of Turkey, 1:500,000 Scale.* General Directorate of Mineral Research and Exploration, Ankara, Publication.

TREUIL, M. & JORON, J.L. 1975. Utilisation des éleménts hygromagmatophiles pour la signification de la modélisation quantitative des processus magmatiques. Examples de l'Afar et dela dorsale médioatlantique. *Italian Society of Mineralogy and Petrology* **31**, 125–174.

TURCOTTE, D.J.L. & EMENNAN, S. H. 1983. Mechanism, of active and passive rifting. *Tectonophysics* **94**, 39–50.

VAUGHAN, A.P.M. & SCARROW, J.H. 2003. K-rich mantle metasomatism in control of localization and initiation of lithospheric strike-slip faulting. *Terra Nova* **15**, 163–169.

WALTER, M.J. 1998. Melting of garnet peridotite and the origin of komatiite and depleted lithosphere. *Journal of Petrology* **39**, 29–60.

WALTER, M.J, SISSON, T.W. & PRESNALL, D.C. 1995. A mass proportion method for calculating melting reactions and applications to melting of model upper mantle lherzolite. *Earth and Planetary Science Letters* **135**, 77–90

WEAVER, B.L. 1991. The origin of ocean island end-member compositions: trace element and isotopic constraints. *Earth and Planetary Science Letters* **104**, 381–397.

WEAVER, B.L. & TARNEY, J. 1984. Empirical approach to estimating the composition of the continental crust. *Nature* **310**, 575–577.

WEINSTEIN, Y., NAVON, O., ALTHERR, R. & STEIN, M. 2006. The role of lithospheric mantle heterogeneity in the generation of Plio–Pleistocene alkali basaltic suites from Harrat Ash Shaam (Israel). *Journal of Petrology* **47**, 1017–50.

WESTAWAY, R. 1994. Present-day kinematics of the Middle East and eastern Mediterranean. *Journal of Geophysical Research* **99**, 12071–12090.

WESTAWAY, R. 2004. Kinematic consistency between the Dead Sea Fault Zone and the Neogene and Quaternary left-lateral faulting in SE Turkey. *Tectonophysics* **391**, 203–237.

WESTAWAY, R. & ARGER, J. 1996. The Gölbaşı basin, southeastern Turkey: a complex discontinuity in a major strike-slip fault zone. *Journal of the Geological Society, London* **153**, 729–743.

WHITE, R.S. & MCKENZIE, D. 1989. Magmatism at rift zones: the generation of volcanic continental margins and flood basalts. *Journal of Geophysical Research* **94**, 7685-7729.

WILSON, M. 1989. *Igneous Petrogenesis.* Unwin Hyman, London.

WITT-EICKSCHEN, G. & HARTE, B. 1994. Distribution of trace elements between amphibole and clinopyroxene from mantle peridotites of the Eifel (western Germany): an ion-microprobe study. *Chemical Geology* **117**, 235–250.

WOOD, D.A. 1979. Dynamic partial melting: its application to the petrogeneses of basalts erupted in Iceland, the Faeroe Islands, the Isle of Skye (Scotland) and the Troodos Massif (Cyprus). *Geochimica et Cosmochimica Acta* **43**, 1031–1046.

WOODLAND, A.B., KORNPROBST, J., MCPHERSON, E., BODINIER, J.L. & MENZIES, M.A. 1996. Metasomatic interactions in the lithospheric mantle: Petrologic evidence from the Lherz Massif, French Pyrenees. *Chemical Geology* **134**, 83–112.

YILMAZ, Y., GÜRPINAR, O. & YİĞİTBAŞ, E. 1988. Tectonic evolution of the Miocene basins at the Amanos Mountains and the Maraş region (in Turkish). *Bulletin of the Turkish Association of Petroleum Geologists* **1**, 52–72.

YURTMEN, S., ROWBOTHAM, G. & FLOYD, P. 2000. Petrogenesis of Quaternary alkali volcanics, Ceyhan-Turkey. *In:* BOZKURT, E., WINCHESTER, J.A., PIPER, J.D.A. (eds), *Tectonics and Magmatism of Turkey and the Surrounding Area.* Geological Society, London, Special Publications **173**, 489–512.

YÜRÜR, T. & CHOROWICZ, J. 1998. Recent volcanism, tectonics and plate kinematics near the junction of African, Arabian and Anatolian plates in the eastern Mediterranean. *Journal of Volcanology and Geothermal Research* **148**, 1–15.

ZINDLER, A. & HART, S.R. 1986. Chemical geodynamics. *Annual Review of Earth Planetary Sciences* **14**, 493–571.

ZOU, H. & ZINDLER, A. 1996. Constraints on the degree of dynamic partial melting and source composition using concentration ratios in magmas. *Geochimica et Cosmochimica Acta* **60**, 711–717.